Modeling Shed Vorticity from Coaxial Blade Interactions

Natasha L. Schatzman* and Ethan A. Romander†
NASA Ames Research Center, Moffett Field, CA, 94035, USA

Narayanan M Komerath‡
Georgia Institute of Technology, Atlanta, GA, 30332, USA

Coaxial counter-rotating rotors operate in a flowfield different from single rotors. Aerodynamic interactions such as blade crossing and shed vorticity result in potential sources of noise and impulsive blade loads. In previous research, the authors simulated two trains of airfoils traveling in opposite directions for specified speeds, airfoil thickness and vertical separation distances, using the compressible Navier-Stokes solver OVERFLOW. Previously, the effects of circulation, thickness, and compressibility were explored. This work continues the previous research by exploring downwash and shed vorticity effects. These phenomena are explored by simulating two trains of eight airfoils vertically separated traveling in opposite directions. The effects of downwash are simulated by introducing a vertical flow. Vorticity shed from the upper train of airfoils is shown to interact with the lower train, affecting the loading on the lower airfoils. Furthermore, viscid and inviscid calculations are performed to further understand the behavior of shed vorticity.

I. Nomenclature

Ai	=	airfoil i
c	=	chord (m)
c_d	=	coefficient of sectional drag
c_l	=	coefficient of sectional lift
c_m	=	coefficient of sectional moment
C_P	=	coefficient of pressure
c_x	=	coefficient of sectional force in the horizontal direction
c_z	=	coefficient of sectional force in the vertical direction
D	=	horizontal separation between airfoils (m)
ISO	=	isolated airfoil
i	=	airfoil number counter (1, 2, 3, 4, ...)
LA	=	lower airfoil
LAi	=	lower airfoil i
M	=	Mach number
M_{tip}	=	tip Mach number
N_b	=	number of blades (per rotor)
R	=	rotor radius (m)
Re	=	Reynolds number ($\rho\, V_\infty\, c/\, \mu$)
r	=	spanwise radial position (m)
r/R	=	dimensionless radial position
S	=	vertical distance between rotors or airfoils (m)
t	=	time (s)
UA	=	upper airfoil
UAi	=	upper airfoil i
V_{eff}	=	effective velocity (m/s)
V_i	=	induced inflow (m/s)

*Aerospace Engineer, Aeromechanics Branch, NASA Ames Research Center, Mail Stop: 243R-11, Moffett Field, CA 94035, USA.
†Aerospace Engineer, Aeromechanics Branch, NASA Ames Research Center, Mail Stop: 243-12, Moffett Field, CA 94035, USA.
‡Professor, Aerospace Engineering, 265 North Ave. NW, Guggenheim-353.

$V_{r/R}$ = velocity at r/R spanwise location (m/s)
V_{tip} = rotor blade rotational speed at tip (m/s)
V_∞ = forward flight velocity (m/s)
α = airfoil angle-of-attack (deg), positive pitch up
Γ = vortex strength (m^2/s^2)
μ = dynamic viscosity of the fluid (N-s/(m^2))
ρ = density in medium (kg/m^3)
θ_{tw} = blade twist angle (deg)
θ_0 = collective pitch angle (deg)

II. Introduction

Coaxial rotor aircraft are gaining interest in civil and military applications, as well as in the small, Unmanned Aerial Vehicle (UAV) market. Studies on coaxial rotor performance through 1997 are summarized in Coleman [1]. Barbely et al. [2] provide a compilation of computational studies of coaxial rotors in hover and forward flight; references for the data used to validate the studies are also cited.

The approach to explore a coaxial rotor in 2D, developed by Schatzman (formerly Barbely) et al. [2–5], was pursued in a recent paper by Singh and Friedmann [6]. Using vortex discretized airfoils, Singh and Friedmann's 2D simulations included effects of downwash and shed vorticity by using periodic boundaries. Furthermore, ongoing coaxial rotor computational and experimental research has been performed by the University of Maryland [7, 8] and University of Texas at Austin [9, 10], with focus on rotor performance and blade flap bending moments, particularly with variation in lift offset.

In a series of studies, Schatzman et al. [2–5] used the OVERFLOW Navier-Stokes solver to model the crossing of two airfoils, offset vertically and traveling in opposite directions in 2D. Vertical spacing between the airfoils, airfoil angle of attack, Mach number (including transonic and compressible cases), and airfoil thickness were varied. The results showed dramatic effects in the aerodynamic loads on the two airfoils, as well as effects on the pressure field surrounding the airfoils during and after the crossing of the two airfoils. In the previous studies [2–5], effects of circulation, thickness, compressibility and shed vorticity were explored, while the effects of downwash were not modeled. Results revealed that circulation was the dominating aerodynamic source compared to thickness and compressibility effects. Schatzman et al. [5] replaced the two-airfoil scenario with a "train" of airfoils, vertically offset, traveling in opposite directions. The train of airfoils is more representative of a coaxial rotor system with each rotor having multiple blades, thus producing numerous blade crossing events in one rotor revolution. The goal was to understand the effect of the shed vorticity of multiple airfoils on the surrounding flowfield and on the airfoil loading.

In this study, the effect of shed vorticity is further investigated, as is the effect of downwash. The addition of downwash gives a more representative simulation to that of a coaxial rotor. Inviscid solutions are analyzed to highlight deposited vorticity at the time of overlap.

III. Method

The effects of shed vorticity and downwash are explored computationally by simulating a coaxial rotor in 2D using airfoils traveling in opposite directions. OVERFLOW is used to calculate inviscid and viscous solutions. Inviscid calculations are performed in order to minimize diffusion of shed vorticity. Furthermore, the induced flow through the rotors, "downwash", is simulated using a vertical freestream velocity to the entire flowfield computed. The downwash vertical velocity is calculated using a Blade Element Momentum Theory code.

A potential flow simulation is used to understand the change in lift at the time of airfoil crossing (or overlap); most of the effects are captured in the incompressible calculation. The potential flow code VITS (Vortex Interaction Tracking Simulation) uses a vortex to simulate the effect of circulation while a source and sink represent the the body of the airfoil for thickness effects.

A coaxial system representative of a modern design [11] is simulated. Table 1 shows the simulated rotor design parameters and the 2D analog.

A. Simulation geometry

In order to understand the effects due to circulation, thickness, compressibility, shed vorticity, and downwash (inflow), multiple simulations were performed to study the effects independently. A complete pictorial list of different

Table 1 Simulated rotor design parameters and 2D analog.

2D analog	value	**Coaxial rotor parameter**	value
Radius (m)	N/A	Radius (m)	6.096
No. of airfoils (per train)	8	N_b (per rotor)	3
S, vertical separation between airfoils (m)	0.6096	S, rotor separation (m)	0.6096
D, horizontal separation between airfoils (m)	12.77	D, arc length between adjacent blade tips (m)	12.77
c, chord (m)	0.1524	c, chord (m)	0.1524
Airfoil speed (m/s)	213.36	Vtip, hover (m/s) r/R=1.0	213.36
M, Mach number	0.627	M, Mach number (M_{tip} for hover)	0.627
Linear twist (deg)	N/A	Linear twist (deg)	-8
α (deg)	5	α (deg)	N/A
θ_0 (deg)	N/A	θ_0 (deg)	0
Airfoils	NACA 0012	Airfoils	varying

types of simulations performed is shown in Fig. 1.

A vertical separation between the upper and lower airfoil train was set equal to the rotor-rotor separation for the coaxial rotor and is described in Table 1. The distance between airfoils in a train (e.g. UA3 and UA4, the third and fourth airfoil in the train) was set equal to the circumferential distance between the tips of the modeled rotor. A train of eight airfoils was chosen to ensure that there was sufficient aerodynamic influence from airfoils preceding and following the airfoil of interest (UA4). The effect of downwash is modeled by a downward velocity.

The time of overlap is when the c/4 of the upper and lower airfoil are aligned. The c_z is the non-dimensional force in the vertical direction at 1/4 chord and c_x is the non-dimensional force in the horizontal direction at 1/4 chord.

B. 2D representation and assumptions

The first step towards understanding this complex 3D time-varying flowfield was to model the coaxial rotor as a 2D potential flow simulation of two airfoils moving past each other. First, a simulation of two airfoils modeled as a source, vortex, and sink were computed to understand effects due to thickness and circulation. Next, a Navier-Stokes computational fluid dynamic tool was used to further investigate incompressible and compressible effects due to circulation, thickness, compressibility, shed vorticity, and downwash (inflow). Unlike a 3D model, the 2D representation did not capture span wise flow, tip vortices, and curvature. Forward flight cases were not investigated in 2D for this analysis.

C. Potential flow simulation

A potential flow simulation was used to understand the change in lift at the time of airfoil crossing (or overlap). A vortex was used in this model to simulate the effect of circulation, while a source and sink were used to represent the body of the airfoil in order to simulate thickness effects. A low-speed incompressible flow is a realistic condition for inboard spanwise radial (r/R) locations.

1. Computational set up

The unsteady effects of two airfoils crossing in an incompressible flow ($M \leq 0.30$) was simulated using the potential flow code VITS (Vortex Interaction Tracking Simulation). VITS, written in MATLAB, was developed to understand the aerodynamic behavior of airfoils crossing at a fixed vertical separation distance, where each airfoil is modeled as a source, vortex, and sink. VITS calculates c_l for each airfoil by using the Biot-Savart law and updating the airfoil's vortex strength for each time step [12]. This simplified model enabled the aerodynamic interactions at the time of an airfoil crossing to be easily analyzed.

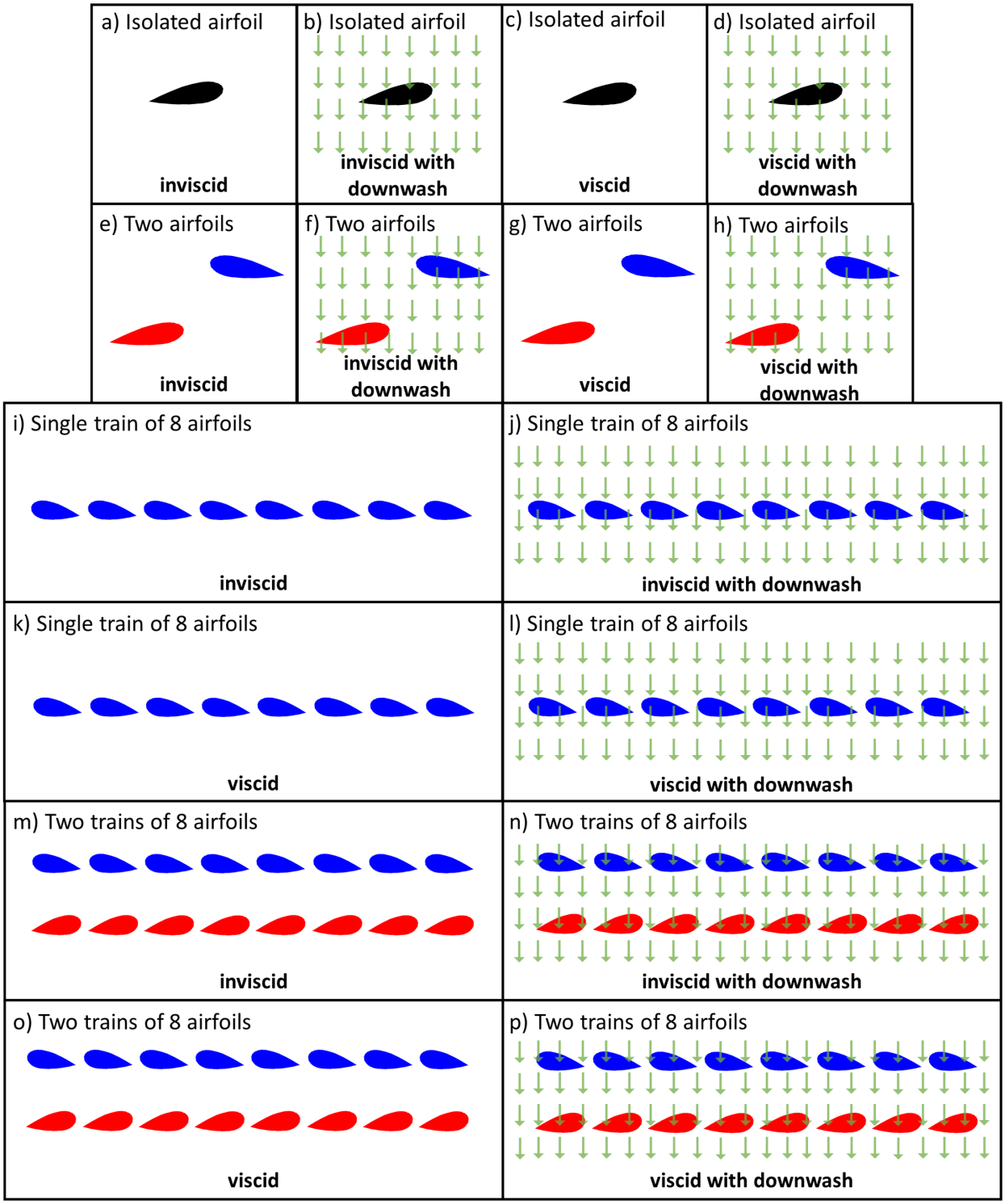

Fig. 1 Inviscid and viscid simulations of an isolated airfoil (a) through d)), two airfoils crossing (e) through h)), train of eight airfoils (i) through l)), and two trains of eight airfoils crossing (m) through p)).

The upper and lower airfoils were each simulated using a source (leading edge), vortex (quarter-chord) and sink (trailing edge) as shown in Fig. 2 a). The source and sink gives the ability to model thickness effects, while the vortex models circulation. Figure 2 b) shows velocity fields of the individual sink, vortex, and source used to represent an airfoil. Figure 2 c) shows a simulated NACA 0012 airfoil at 9.8 degree angle-of-attack traveling at $M = 0.25$ using the source-vortex-sink model. The simulated airfoils are representative of a NACA 0012 with a chord of 0.1524 m. For the simulation of two airfoils crossing, the vertical separation distance was two chords. Since airfoil geometry was not fully modeled, only the change in angle-of-attack caused by the two airfoils crossing was analyzed.

D. Compressible simulation

OVERFLOW 2.2k [13], a compressible Reynolds-Averaged Navier-Stokes solver, was used to simulate the 2D cases for viscous and inviscid calculations.

1. OVERFLOW

OVERFLOW 2.2k [13], developed by NASA, is a compressible Reynolds-Averaged Navier-Stokes CFD analysis tool that uses structured, overset grids. This study used OVERFLOW's 2D configuration to model airfoils moving through a static background mesh. Over the course of the simulation, these airfoil(s) converged horizontally toward the origin at a speed representative of the tip speed of the coaxial rotor design. At the origin they passed by each other to model a blade passage or "overlap." The upper airfoil(s) were initially displaced 200 chord lengths to the right of the origin while the lower airfoils were initially displaced 200 chord lengths to the left of the origin. This distance was chosen to give the flow sufficient time to reach a steady state before the airfoil grids reached the origin. The airfoils were also displaced from the origin in the vertical axis by a distance that represented the rotor-rotor separation for the given coaxial design. This vertical separation was held constant for the entire simulation.

OVERFLOW 2.2k offers a wide variety of numerical schemes, turbulence models, and boundary conditions. All simulations in this study used 5th-order accurate central differencing of the Euler terms and a 3rd-order accurate Beam-Warming block-diagonal scheme with Steger-Warming flux split Jacobians for the diffusion terms. This arrangement is formally 3rd-order accurate in space. Time marching was performed using a 2nd-order dual time stepping scheme. For viscous simulations turbulence was modeled using the Spalart-Allmaras one-equation turbulence model and airfoil surfaces were modeled as no-slip, adiabatic walls. Inviscid simulations modeled the airfoils as adiabatic walls with enforced flow tangency. The edges of the computational domain were modeled using a characteristic condition that imposed a $M = 0.05$ freestream vertically downward at standard atmospheric conditions. This small freestream velocity was used to stabilize vorticity in the solution and to provide some modeling of induced velocity through the coaxial rotor disks for "downwash" cases only. A physical time step was chosen such that the airfoils moved 1/200th of a chord length for each time step. Each physical time step included 20 Newton subiterations. These values ensured that subiteration convergence met or exceeded two orders of decrease in the residual at all times.

Airfoils were modeled using a set of identical body fitted, curvilinear structured grids. These grids were of an O-topology with 253 points around each airfoil and 65 points normal to the airfoil surface. The y+ value at the first point off the airfoil surface was less than one. These airfoil grids moved through a Cartesian background mesh that extended 1200 chords from the origin in the horizontal and vertical direction. Background grids can be refined based on an estimate of the solution error using overlapping Cartesian refinement grids (see Fig. 3). This grid adaption scheme ensured sufficient grid support for shed vorticity in the wake of the airfoils. All grids were modeled in 2D. Total grid sizes ranged from approximately 350,000 points for an isolated airfoil before grid adaption to approximately 11 million for an eight-airfoil simulation after grid adaption.

Forces and moments exerted on the airfoils were integrated from the pressure and viscous stress at the airfoil surface. These quantities were integrated and recorded periodically over the entire course of the simulation. The force in the vertical (z) direction is positive up and is equivalent to aerodynamic lift. The coefficient of z-force is abbreviated as c_z. The direction of force in the horizontal (x) direction is positive toward the airfoil's trailing edge and is equivalent to aerodynamic drag. The coefficient of x-force is abbreviated by c_x. Atmospheric conditions for all 2D OVERFLOW simulations are seen in Table 2.

2. Blade Element Momentum Theory

The induced velocity (downwash) was calculated using a Blade Element Momentum Theory (BEMT) hover model for the modern rotor design as shown in Table 1. The results from the BEMT hover model were then compared to

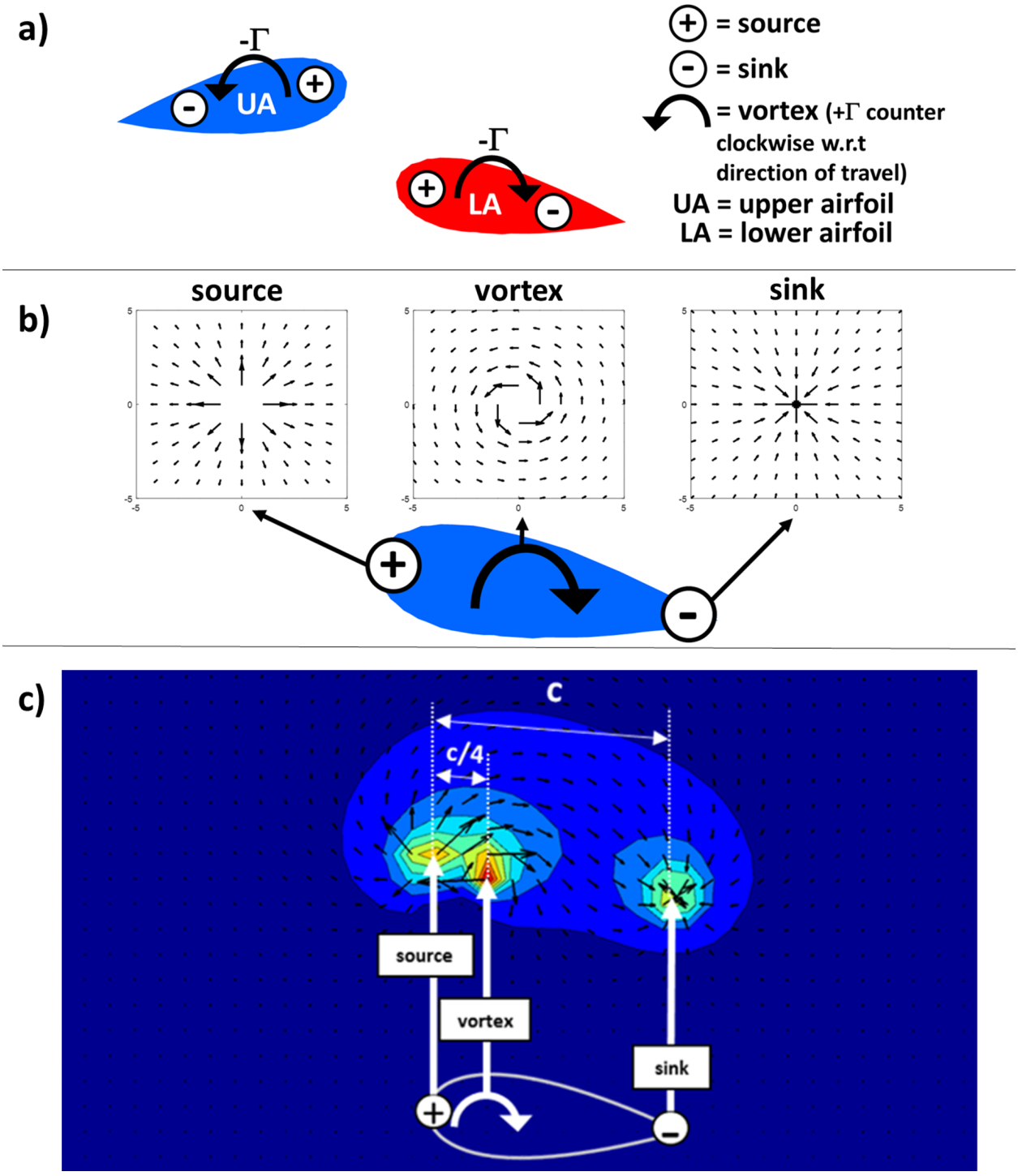

Fig. 2 a) Pictorial representation of two airfoils moving past each other modeled by a source, sink, and vortex, b) mathematical model of an individual sink, vortex, and source and c) simulation of a combined sink, vortex, and source for an isolated airfoil.

Table 2 Atmospheric conditions for 2D OVERFLOW simulations.

Variable	Value	Units
pressure	101325	(Pa)
dynamic viscosity (viscous)	1.7965×10^{-5}	(kg/(m-s))
density	1.225	(kg/m^3)
temperature	288.2	(K°)
speed of sound	343	(m/s)

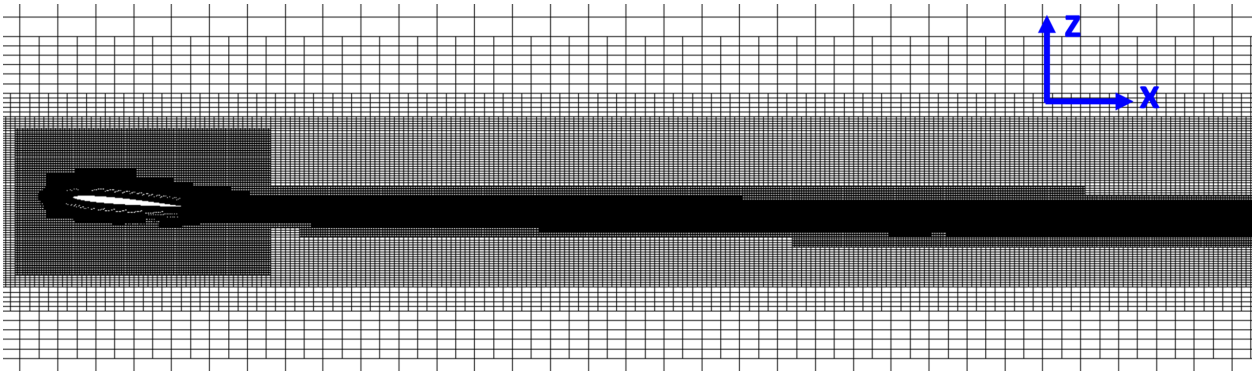

Fig. 3 OVERFLOW 2.2k simulation with grid adaption for an NACA 0012 isolated airfoil at α = 5°.

CAMRAD II calculations [14] as shown in Fig. 4. The BEMT uses a coaxial interference-induced power factor from Leishman's Case 4a [15]. Leishman's Case 4a assumes that the rotors have balanced torque with the lower rotor operating in the slipstream of the upper rotor. The BEMT uses a C81 table and interpolates to find the correct C_l and C_d for the various span locations. For all OVERFLOW downwash simulations, an induced velocity (V_i) of 9.45 m/s was used from the modern rotor design BEMT results.

IV. Potential flow simulation results

As the two airfoils approach each other, each airfoil induces a velocity on the other, resulting in a change in vortex strength. Figure 5 shows c_l versus distance to overlap for a flight condition of $M = 0.25$, $\alpha = 9.8°$, and $S/c = 4.0$ (S = 0.6096 m, c = 0.1524 m) without downwash for upper and lower airfoil. The c_l of the upper (UA) and lower (LA) airfoils for VITS calculations see an increase in lift before overlap followed by a decrease in lift after overlap. To understand the change in c_l before and after overlap, the flowfield is analyzed.

Figure 6 shows the flowfield from the VITS simulation in terms of vorticity for two airfoils before, at, and after the time of crossing at a flight condition of $M = 0.25$, $\alpha = 9.8°$, and $S/c = 4.0$ (S = 0.6096 m, c = 0.1524 m). To simplify the problem, downwash was not modeled for this simulation, but will be explored using OVERFLOW in a later section. As the two airfoils approach each other, the surrounding flowfield of each airfoil begins to interact. The interaction causes a symmetrical flowfield before, at, and after time of overlap due to the absence of viscosity, resulting in an equal and opposite change in lift for the upper and lower airfoil. The resultant time history of the change in angle-of-attack (or lift) and induced velocity is visually explained in Fig. 7. When compressibility is not dominating, the lift of both the upper and lower airfoil increases before the overlap, followed by a decrease in lift after the overlap. Before the overlap, the upper airfoil sees an increase in angle-of-attack due to the upwash from the lower airfoil. The angle-of-attack of the lower airfoil also increases due to the upwash from the upper airfoil. Therefore an increase in lift is experienced by both airfoils as depicted in Fig. 7 a). The opposite occurs after the time of the overlap, where the lift for both the upper and lower airfoils (see Fig. 7 b)) decreases. As the airfoils approach one another, c_l of each airfoil changes due to the circulation effect of the other airfoil. A compressible flow solver is needed to further investigate the effects of viscosity, circulation, thickness, compressibility, downwash, and shed vorticity.

In Fig. 8 the change in airfoil circulation with time ($-d\Gamma/dt$) was calculated from the airfoil lift time history in order

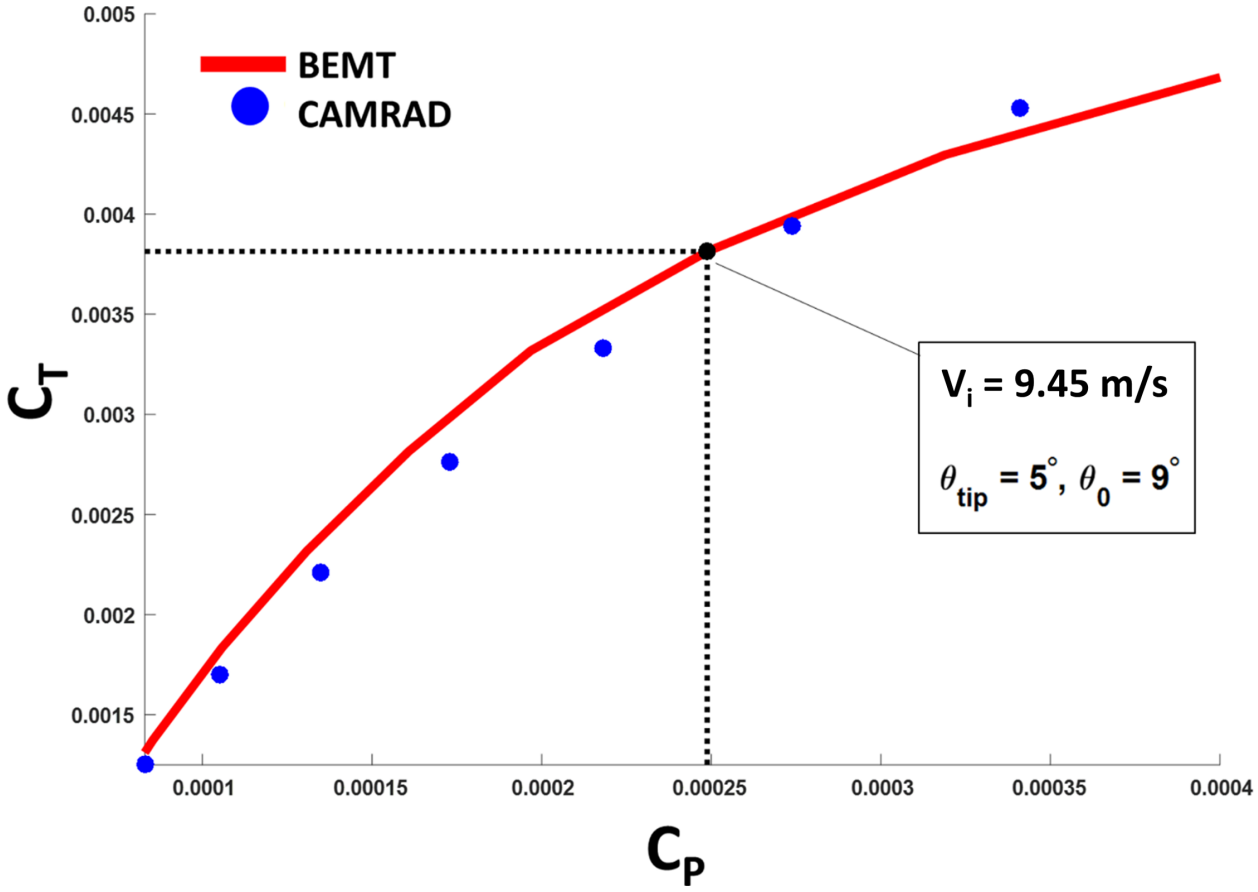

Fig. 4 Coefficient of thrust versus coefficient of power for modern coaxial rotor in hover.

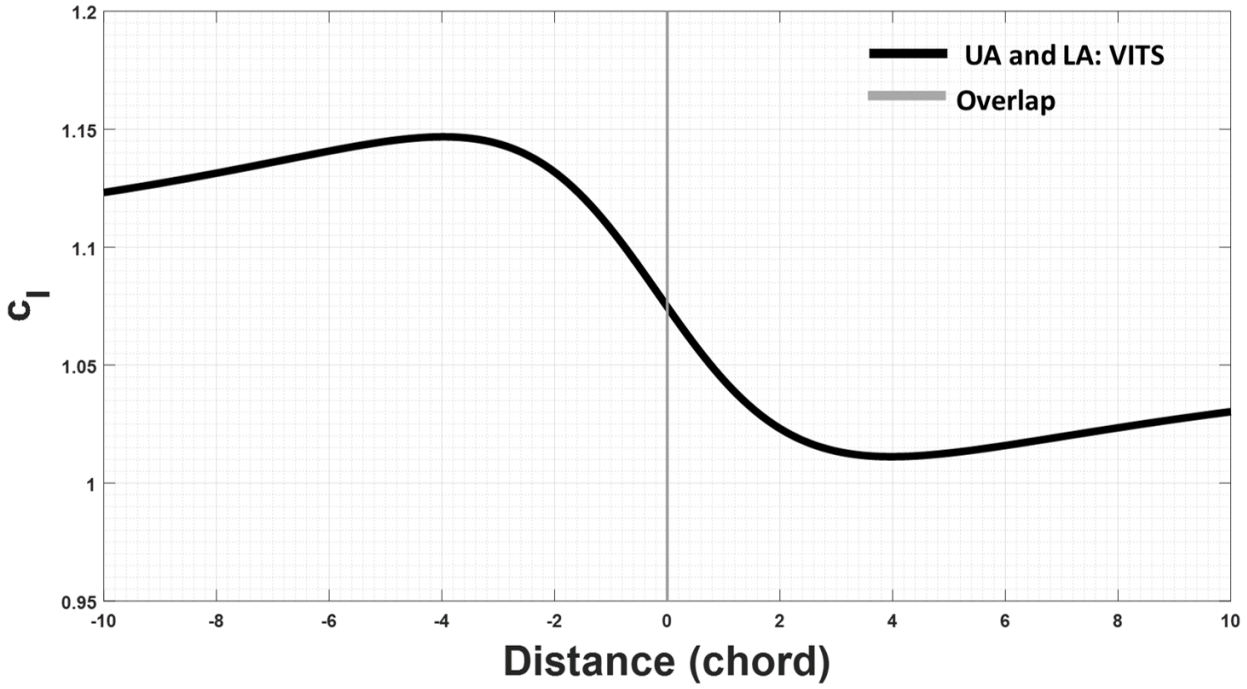

Fig. 5 VITS simulation of two airfoils crossing, c_l versus distance to overlap in chords (M = 0.25, α = 9.8°, and S/c = 4.0 (S = 0.6096 m, c = 0.1524 m)).

to investigate shed vorticity for Harrington Coaxial rotor 1 (HC1) [16]. The HC1 was modeled in the previous work by Schatzman (formerly Barbely) et al. [2–5]. The circulation calculations were first performed for an isolated airfoil and the upper airfoil (UA) of a two airfoil simulations, as shown in Fig. 8 (HC1: M = 0.47 (V_{tip} = 152.4 m/s), α = 7°, and S/c = 6.21 (S = 0.7102 m, c = 0.1143 m)). The horizontal axis is in terms of chord distance to overlap; negative and positive values correspond to before and after airfoil overlap, respectively. The vertical gray line is the location where the quarter-chord of the upper and lower airfoils overlap. The c_z results are converted to circulation (Γ) (Fig. 8 b)), then the negative time derivative of circulation is computed to obtain shed vorticity ($-d\Gamma/dt$) (Fig. 8 c)). The circulation is negated to satisfy Kelvin's circulation theorem (conservation of body forces), and the derivative of circulation is taken with respect to time (distance) due to the time varying loads. There is an increase in shed vorticity beginning about ten chords before overlap, peaking just before overlap, and then decreasing back to zero approximately ten chords after overlap. In order to simulate the effect of shed vorticity, a train of airfoils is modeled to investigate the impact of deposited shed vorticity on an airfoil in the middle of the train (analogous to a rotor with multiple blades).

V. Compressible simulation results

OVERFLOW 2.2k was used to calculate the compressible solutions for both inviscid and viscid cases. The inviscid and viscid isolated airfoil solutions are denoted by "$ISO_{Inviscid}$" and "ISO_{Viscid}", respectively. For two airfoils crossing, inviscid and viscid solutions are denoted by "$UA_{Inviscid}$" and "UA_{Viscid}" for the upper airfoil and "$LA_{Inviscid}$" and "LA_{Viscid}" for the lower airfoil, respectively. For the multiple airfoil crossing simulation inviscid and viscid solutions are denoted by "$UAi_{Inviscid}$" and "UAi_{Viscid}" for the upper airfoil and "$LAi_{Inviscid}$" and "LAi_{Viscid}" for the lower airfoil, respectively, where "i" denotes which number airfoil in the train (i=1-8). The effect of shed vorticity is first presented followed by the effect of downwash.

A. Shed vorticity and downwash

The two airfoils traveling in opposite directions demonstrated the effects of circulation, thickness, and compressibility for a coaxial rotor, but lacked any effect of the rotor wake due to multiple blades. Viscous effects due to shed vorticity

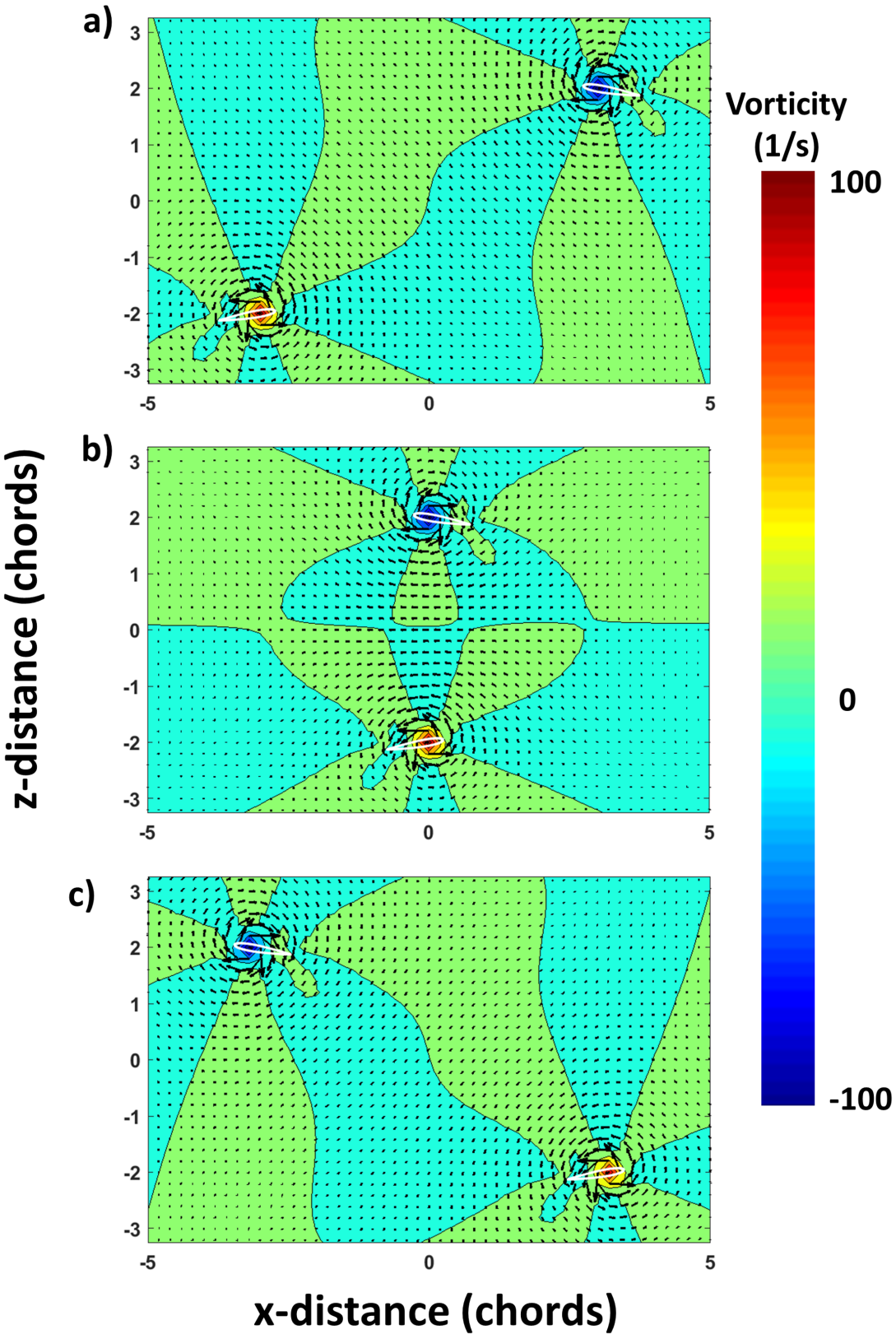

Fig. 6 Simulation of two airfoils using VITS: a) before, b) at, and c) after time of crossing. Vorticity contour shown with u and v velocity vectors, downwash not simulated. (M = 0.25, α = 9.8°, and S/c = 4.0 (S = 0.6096 m, c = 0.1524 m)).

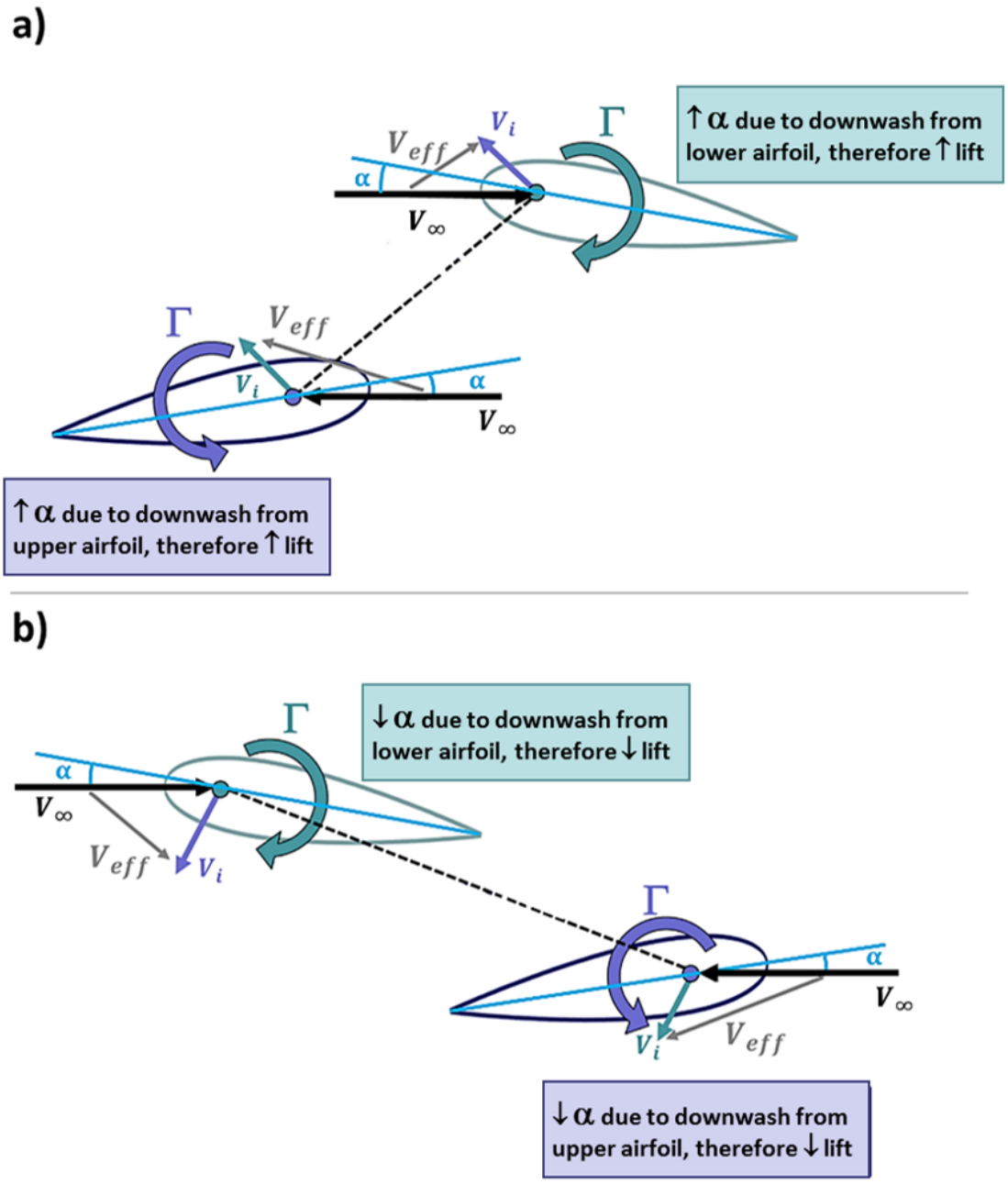

Fig. 7 Change in lift of two NACA 0012 (when compressibility is not dominating) airfoils crossing: a) before and b) after.

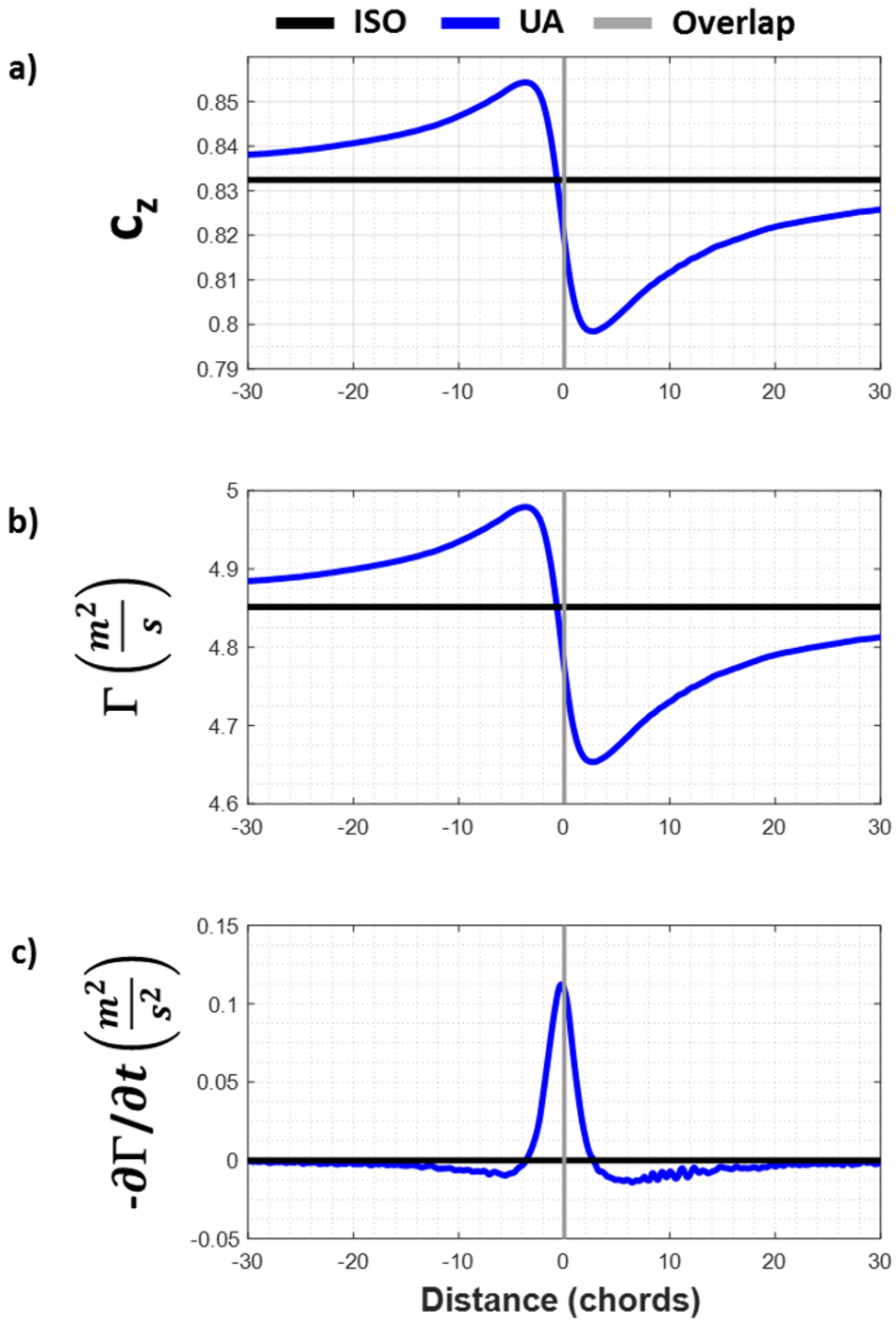

Fig. 8 Results for an isolated airfoil and the upper airfoil of the two airfoils crossing case a) c_z**, b)** Γ**, and c)** $-d\Gamma/dt$**. Horizontal axis is distance to overlap for the upper airfoil (UA) (HC1:** M **= 0.47 (**V_{tip} **= 152.4 m/s),** α **= 7°, and** S/c **= 6.21 (**S **= 0.7102 m,** c **= 0.1143 m)).**

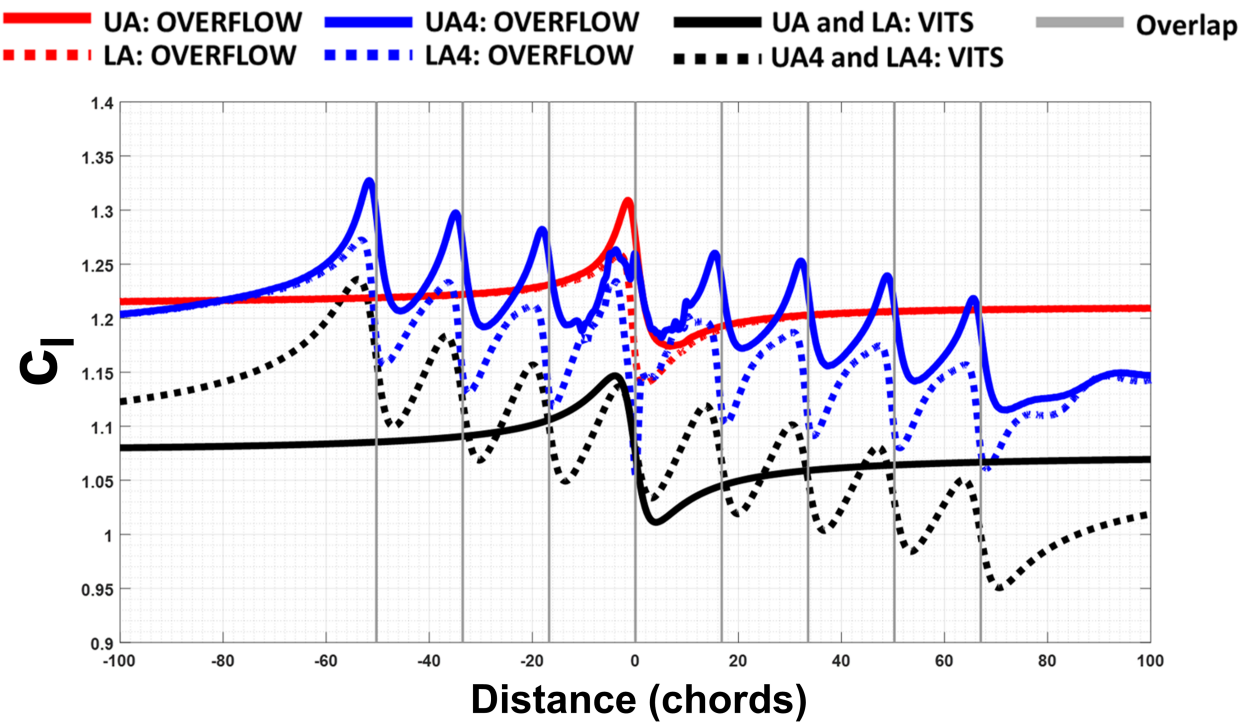

Fig. 9 VITS (inviscid) and OVERFLOW (inviscid) calculations of two airfoils and two trains of eight airfoils crossing, c_l versus distance to overlap in chords (M = 0.25, α = 9.8°, and S/c = 4.0 (S = 0.6096 m, c = 0.1524 m), and D/c = 33.51).

and downwash are discussed by comparing the aerodynamic flowfield of an isolated airfoil, two airfoils crossing, a single train of eight airfoils, and two trains of eight airfoils crossing. Inviscid calculations were performed to reveal further information that may not be easily discerned from viscous calculations.

For this study, a configuration was introduced that is representative of modern coaxial systems [11], and previously modeled by Barbely et al. [2–4]. The modern coaxial rotor design has three blades per rotor, a smaller rotor-rotor vertical separation distance, and faster tip speed compared to the the HC1. Table 1 shows the modern coaxial rotor design parameters and the 2D analog.

The downwash was simulated by introducing a vertical velocity everywhere as shown in Figs. 1 b), d), f), h), j), l), n), and p). As previously mentioned, a downwash (V_i) of 9.45 m/s was used from the modern rotor design BEMT results, as shown in in Fig. 4.

As previously shown in Figs. 5 and 6, two airfoils crossing investigated effects due to circulation. VITS was used to investigate shed vorticity by simulating a train of eight airfoils traveling in opposite directions. Results are compared to OVERFLOW simulations as shown in Fig. 9. Comparing VITS simulations for UA/LA and $UA4/LA4$, the addition of airfoils resulted in a change in lift for $UA4$ and $LA4$ due to the circulation and crossing interaction of the surrounding airfoils, which was accounted for by using the Biot-Savart law [12]. Inviscid OVERFLOW calculations resulted in higher lift compared to the inviscid VITS potential calculations, this is due to the difference in airfoil modeling. OVERFLOW models the geometry, while VITS uses a source, vortex, and sink to represent an airfoil. The flight condition and geometry used to explore viscosity, shed vorticity, and downwash effects are based on a modern rotor design at a span location of r/R = 0.40, where M = 0.25, α = 9.8°, and S/c = 4.0 (S = 0.6096 m, c = 0.1524 m), and D/c = 33.51 (see Table 3).

Viscosity was not represented in VITS calculations. To visualize shed vorticity, OVERFLOW y-vorticity contours are used to analyze the flowfield. Inviscid flowfield disturbances dissipate at a slow rate, because of this the shed vorticity can be preserved and further analyzed. Each effect and simulation is discussed and compared in terms of c_z, c_x, and c_m versus distance to airfoil overlap, coefficient of pressure contour (C_P), and y-vorticity contour.

The vertical separation distance of the two airfoils is equal to the vertical distance between the two rotors of a coaxial

Table 3 2D representation of a coaxial and single rotor r/R location.

r/R	R (m)	D/c	$V_{r/R}$ (m/s)	M	θ_{tw} (°)	α (°)	Re #
0.13	0.82	11.14	28.38	0.08	4.94	11.94	3.0x10^5
0.25	1.52	20.94	53.34	0.16	4.00	11.00	5.6x10^5
0.40	2.44	33.51	85.34	0.25	2.80	9.80	8.9x10^5
0.50	3.05	41.89	106.68	0.31	2.00	9.00	1.1x10^6
0.60	3.66	50.27	128.02	0.38	1.20	8.20	1.3x10^6
0.75	4.57	62.83	160.02	0.47	0.00	7.00	1.7x10^6
0.80	4.88	67.02	170.69	0.50	-0.40	6.60	1.8x10^6
0.85	5.18	71.21	181.36	0.53	-0.80	6.20	1.9x10^6
0.90	5.49	75.40	192.02	0.56	-1.20	5.80	2.0x10^6
0.95	5.79	79.59	202.69	0.60	-1.60	5.40	2.1x10^6
1.00	6.10	83.78	213.36	0.63	-2.00	5.00	2.2x10^6

Fig. 10 Multiple airfoil simulation illustration at time of overlap of $UA4$ and $LA4$.

rotor. To model the blade phase angle in 2D, the distance between two airfoils (e.g. $UA3$ and $UA4$) was set to the circumferential distance between adjacent blade the tips (or specified r/R location) of the modeled rotor. A total of eight airfoils was simulated and the 4th airfoil in the trains ($UA4$ and $LA4$) was chosen to ensure that the aerodynamic influence from the airfoils ahead and behind were captured. Further investigation regarding the total number of airfoils is necessary to ensure a converged solution for the middle airfoil in the train. This was not performed in this work.

Figure 10 shows a train of eight airfoils representing the upper rotor blades and eight airfoils representing the lower rotor blades. Airfoils are labeled by vertical position (upper or lower) and horizontal position. For example, upper airfoil four and lower airfoil four are denoted as $UA4$ and $LA4$. Figure 10 shows the positions of a multiple airfoil simulation when $UA4$ and $LA4$ are overlapped (the quarter-chord location of each airfoil coincide). All results shown are when $UA4$ and $LA4$ are overlapped. The full time history for the multiple viscid airfoil simulation $UA4$ and $LA4$ over time with labeled crossings (M = 0.25, α = 9.8°,V_i = 9.45 m/s, S/c = 4.0 (S = 0.6096 m, c = 0.1524 m), and D/c = 33.51) are shown in Fig. 11. By the time $UA4$ and $LA4$ overlap, $UA4$ has already overlapped with $LA1$ through $LA3$, while $LA4$ has overlapped with $UA1$ through $UA3$.

Figure 12 shows viscid and inviscid isolated airfoil, two airfoils crossing at crossing (UA/LA), single train of eight airfoils ($A4$), and two trains of eight airfoils at crossing ($UA4/LA4$) with and without downwash for c_z versus distance (M = 0.25, α = 9.8°,V_i = 9.45 m/s, S/c = 4.0 (S = 0.6096 m, c = 0.1524 m), and D/c = 33.51). Figures 13 and 14 show c_x and c_m versus distance for the same condition for viscid simulations only. For the same conditions, the flowfield in terms of C_P contour are shown in Fig. 15 for the isolated airfoil, single train of eight airfoils, and at the time of crossing of two airfoils and a train of eight airfoils crossing simulation. The C_P contour reveals a clear difference between the isolated airfoil and single train of airfoils simulations (Figs. 15 a) through d) and Figs. 15 i) through l)) compared to the simulations with crossing events (Figs. 15 e) through h) and Figs. 15 m) through p)), where the flowfields of the oncoming airfoil(s) coincide. Further investigation of the flowfield is performed to understand the effects of downwash and shed vorticity.

All the different simulations (isolated airfoil, single train of eight airfoils, and at the time of crossing of two airfoils

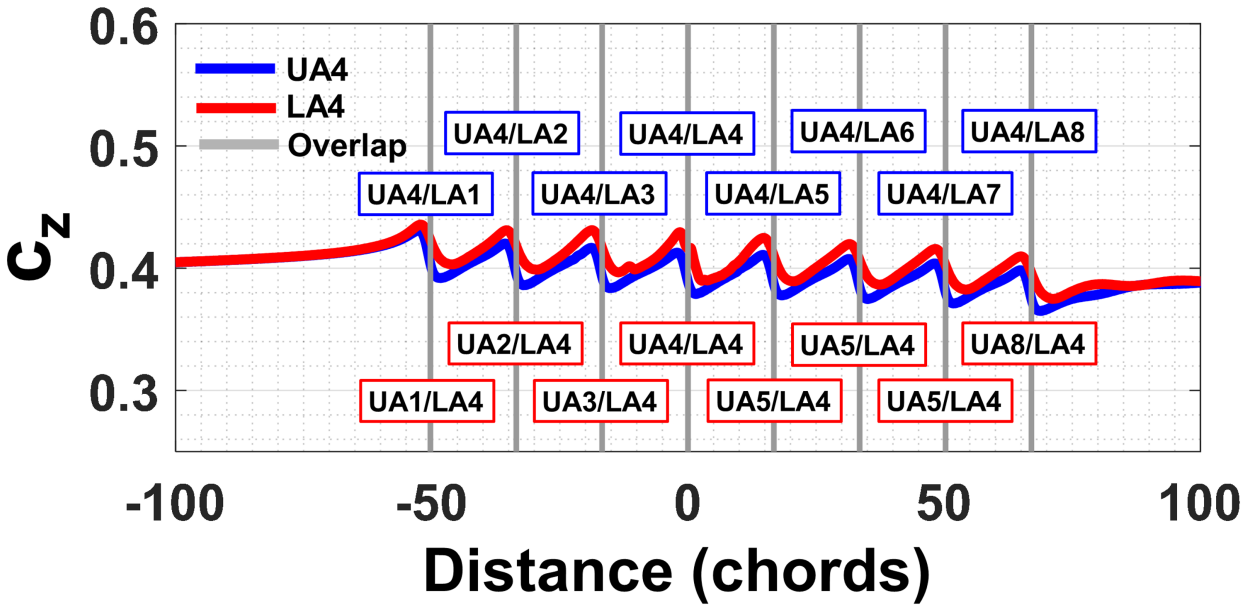

Fig. 11 Two trains of eight airfoils crossing viscid airfoil simulation $UA4$ and $LA4$ for c_x versus distance to overlap of $UA4$ and $LA4$ with downwash (M = 0.25, α = 9.8°,V_i = 9.45 m/s, S/c = 4.0 (S = 0.6096 m, c = 0.1524 m), and D/c = 33.51).

and a train of eight airfoils crossing), with or without downwash, showed an increase in c_z versus distance (Fig. 12) for the inviscid simulations compared to the viscid simulations. Lift is higher for the inviscid calculations due to the absence of a boundary layer. Inviscid solutions for c_x and c_m are negligible due to the absence of viscosity and are not shown in Figs. 13 and 14.

1. Isolated airfoil

As shown in Figs. 12 through 14 for an isolated airfoil, a larger lift is observed for inviscid calculations compared to viscous calculations. For an isolated airfoil, C_P and y-vorticity contours are shown in Figs. 15 a) through d) and 16 for a) viscid without downwash, b) viscid with downwash, c) inviscid, without downwash, and d) inviscid, downwash simulation (M = 0.25 (V_{tip} = 85.34 m/s), α = 9.8°, V_i = 9.45 m/s).

The pressure above the viscid and inviscid isolated airfoils without downwash (Figs. 15 a) and c)) is lower compared to the simulations with downwash (Figs. 15 b) and d)), while below the inviscid airfoils without downwash the pressure is larger compared to the simulations with downwash, because of this lift for viscid and inviscid airfoils without downwash is greater. The simulated downwash decreased overall lift for the inviscid and viscid solution and increased drag for the viscid simulation. Little information between the viscid and inviscid airfoils without downwash simulations (Figs. 15 a) and c)) can be discussed, and as such the y-vorticity contour of the flowfield is analyzed.

The y-vorticity contour further reveals the differences between the inviscid and viscid without (Figs. 16 a) and c)) and with downwash (Figs. 16 b) and d)) simulations. The inviscid and viscid simulation with downwash shows a slowly descending wake sheet at the trailing edge of the airfoil compared to the simulation without downwash. This is due to the vertical velocity (V_i) of 9.45 m/s. Viscid solutions have higher y-vorticity due to the presence of a boundary layer (viscosity). Furthermore, the addition of downwash decreases lift, the vertical velocity decreases the angle-of-attack causing an decrease in lift while drag and moment is increased.

2. Two airfoils crossing

A second airfoil traveling in the opposite direction was added to the isolated airfoil simulation. Compared to the isolated airfoil results, all simulations of two airfoils crossing show a change in c_z, c_x, and c_m before and after time of overlap (Figs. 12 through 14). The change in c_z, c_x, and c_m is caused by the interaction of the flowfields of each airfoil.

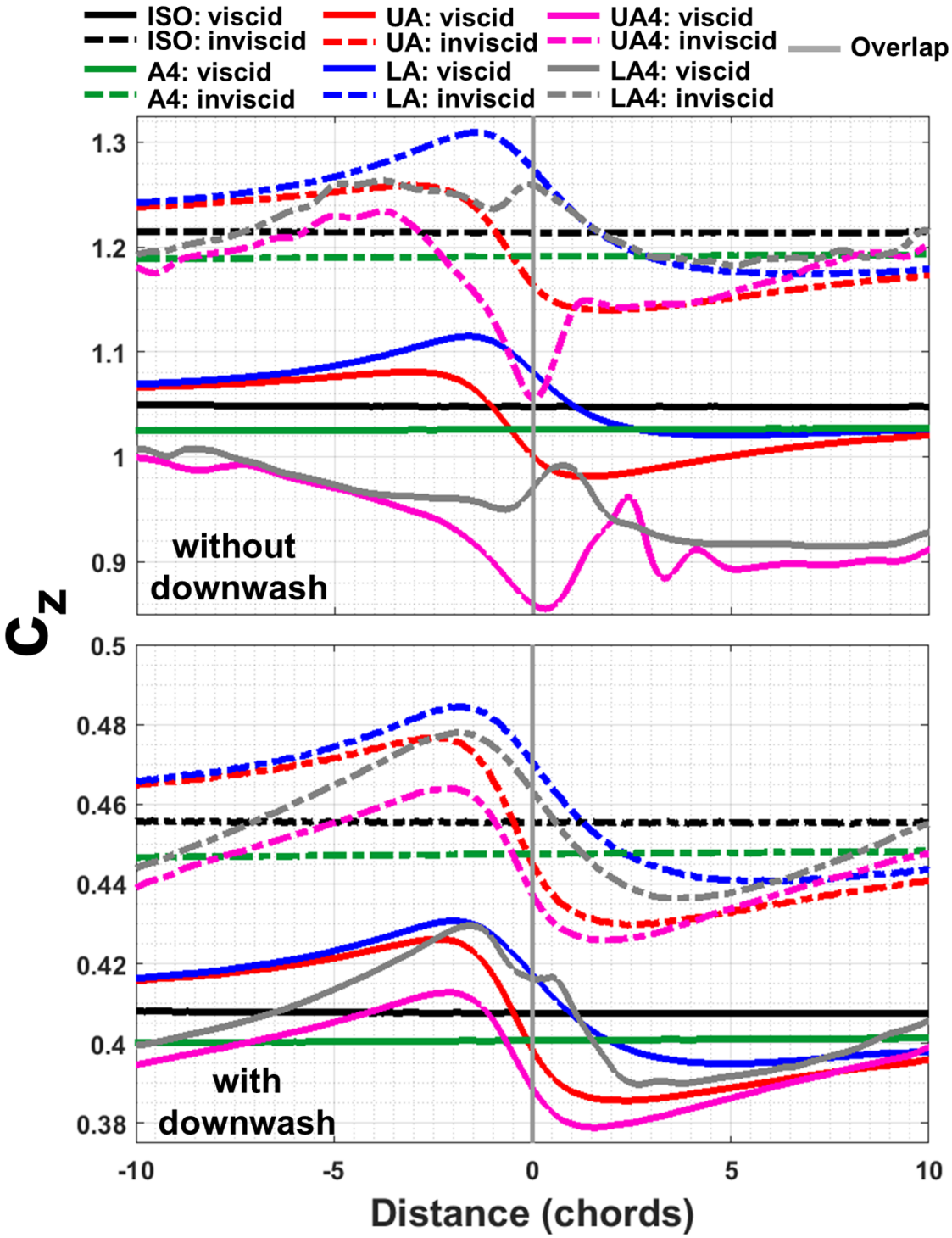

Fig. 12 A viscid and inviscid isolated airfoil, two airfoils crossing at crossing (UA/LA), a single train of eight airfoils ($A4$), and two trains of eight airfoils at crossing ($UA4/LA4$) with and without downwash c_z versus distance (M = 0.25, α = 9.8°, V_i = 9.45 m/s, S/c = 4.0 (S = 0.6096 m, c = 0.1524 m), and D/c = 33.51).

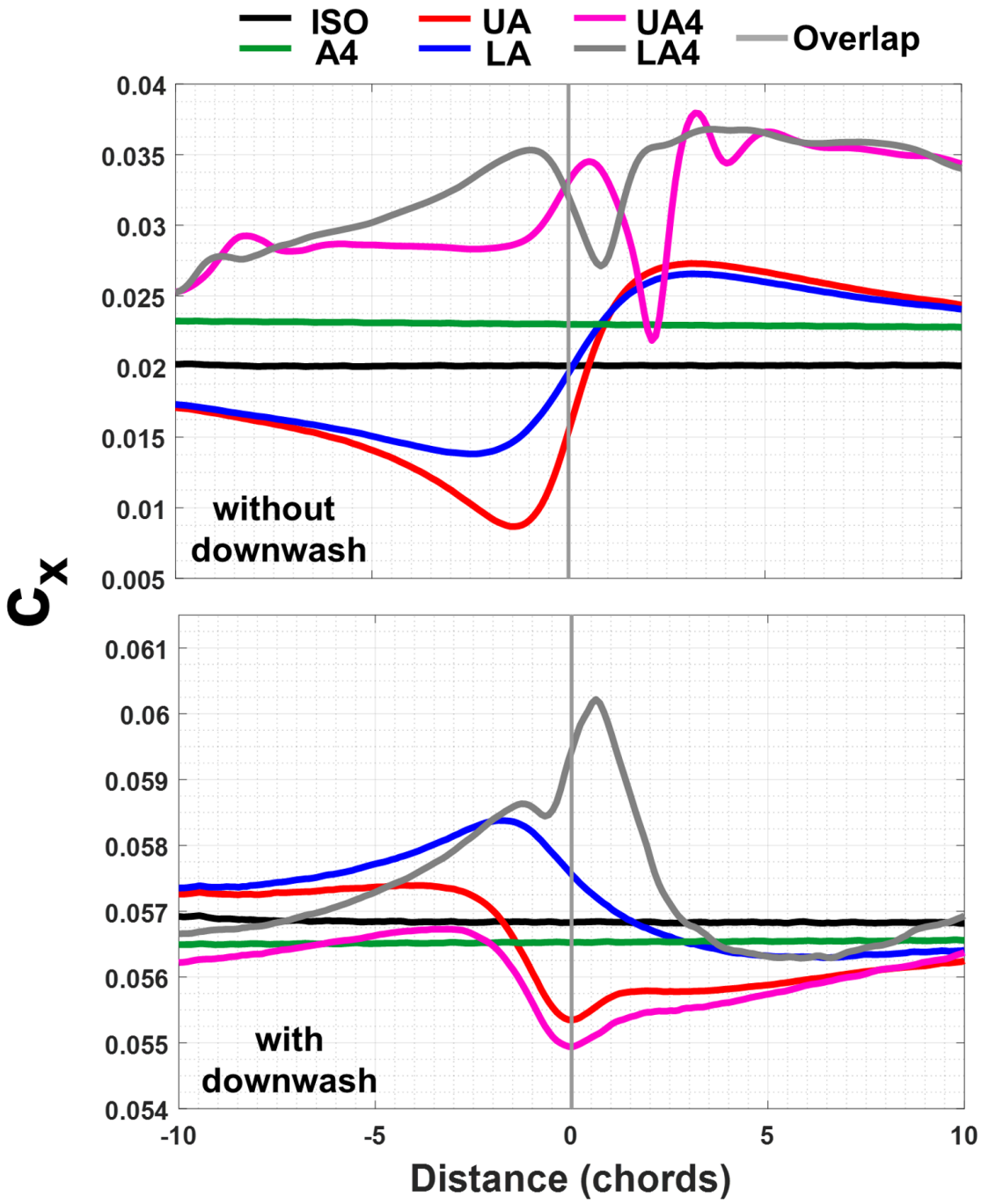

Fig. 13 Isolated airfoil, two airfoils crossing at crossing (UA/LA), a single train of eight airfoils ($A4$), and two trains of eight airfoils at crossing ($UA4/LA4$) with and without downwash c_x versus distance (M = 0.25, α = 9.8°, V_i = 9.45 m/s, S/c = 4.0 (S = 0.6096 m, c = 0.1524 m), and D/c = 33.51). All solutions are viscous.

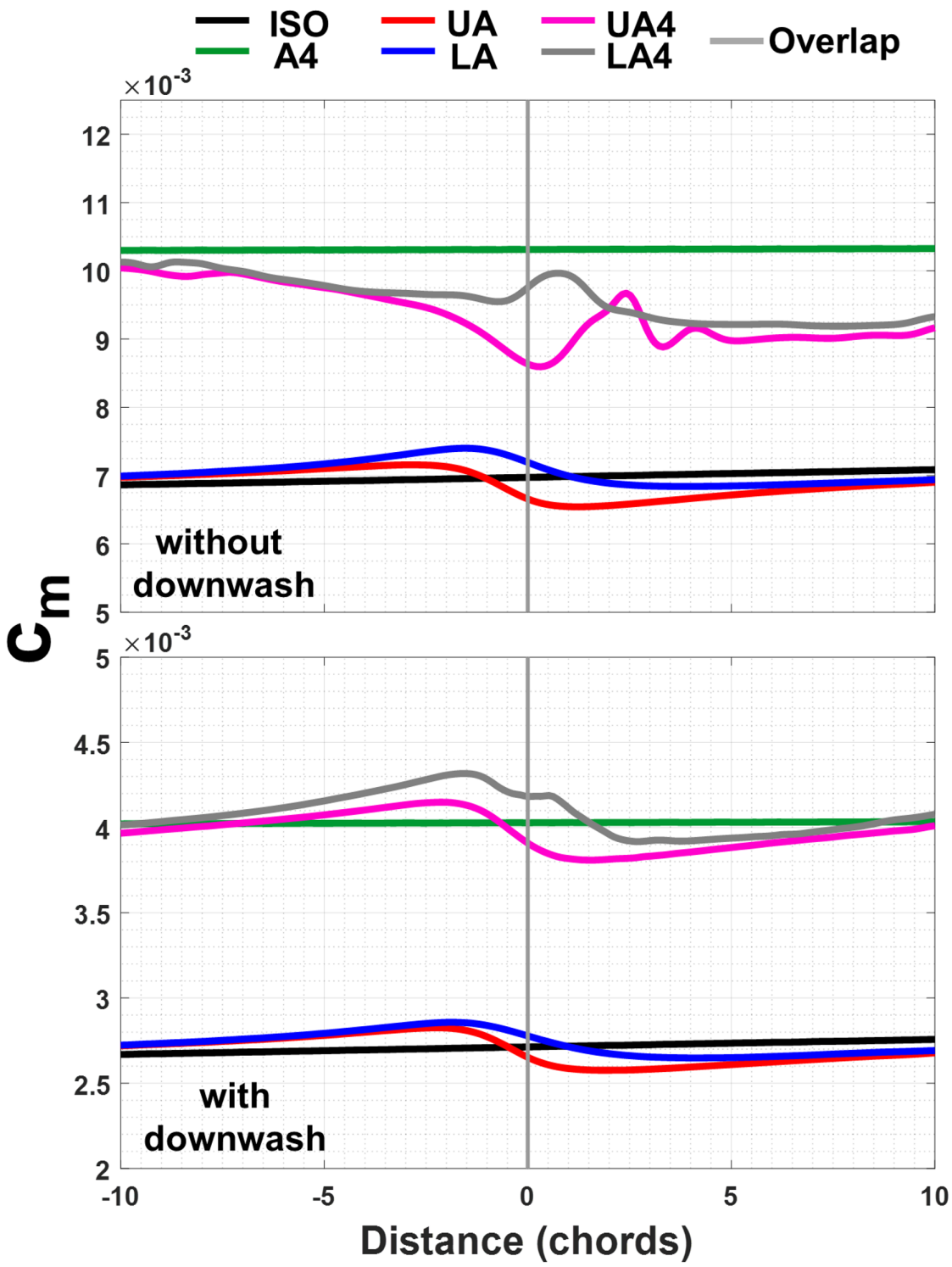

Fig. 14 Isolated airfoil, two airfoils crossing at crossing (UA/LA), a single train of eight airfoils ($A4$), and two trains of eight airfoils at crossing ($UA4/LA4$) with and without downwash c_x versus distance (M = 0.25, α = 9.8°, V_i = 9.45 m/s, S/c = 4.0 (S = 0.6096 m, c = 0.1524 m), and D/c = 33.51). All solutions are viscous.

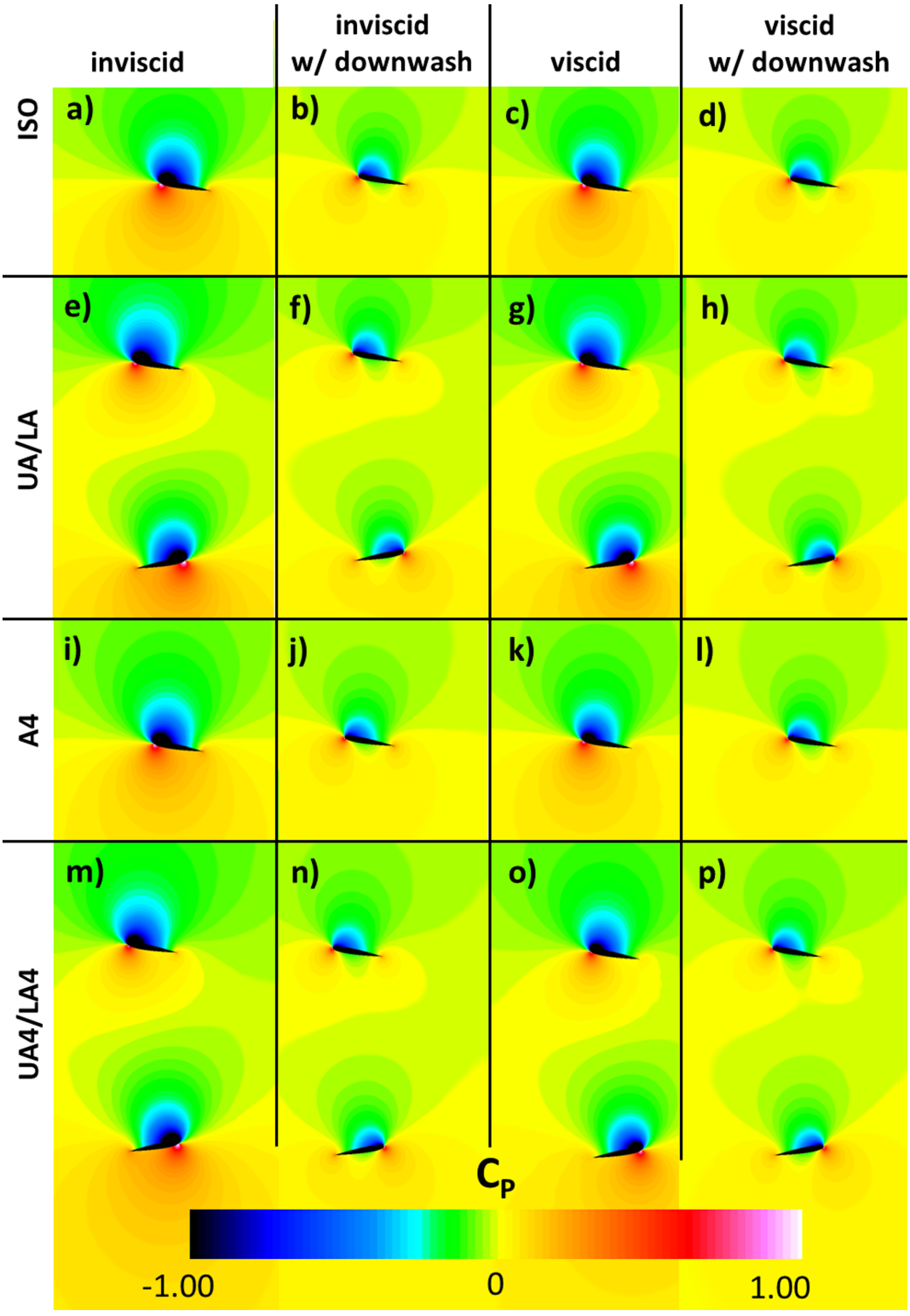

Fig. 15 An isolated airfoil, two airfoils crossing at crossing (UA/LA), a single train of eight airfoils ($A4$), and two trains of eight airfoils at crossing ($UA4/LA4$). Condtions are for inviscid flow without downwash (a), e), i), and m)), inviscid with downwash (b), f), j), and n)), viscid without downwash (c), g), k), and o)), and viscid with downwash (d) h) i) and p)), C_P contours (M = 0.25 (V_{tip} = 85.34 m/s), α = 9.8°, V_i = 9.45 m/s, and S/c = 4.0 (S = 0.6096 m, c = 0.1524 m)).

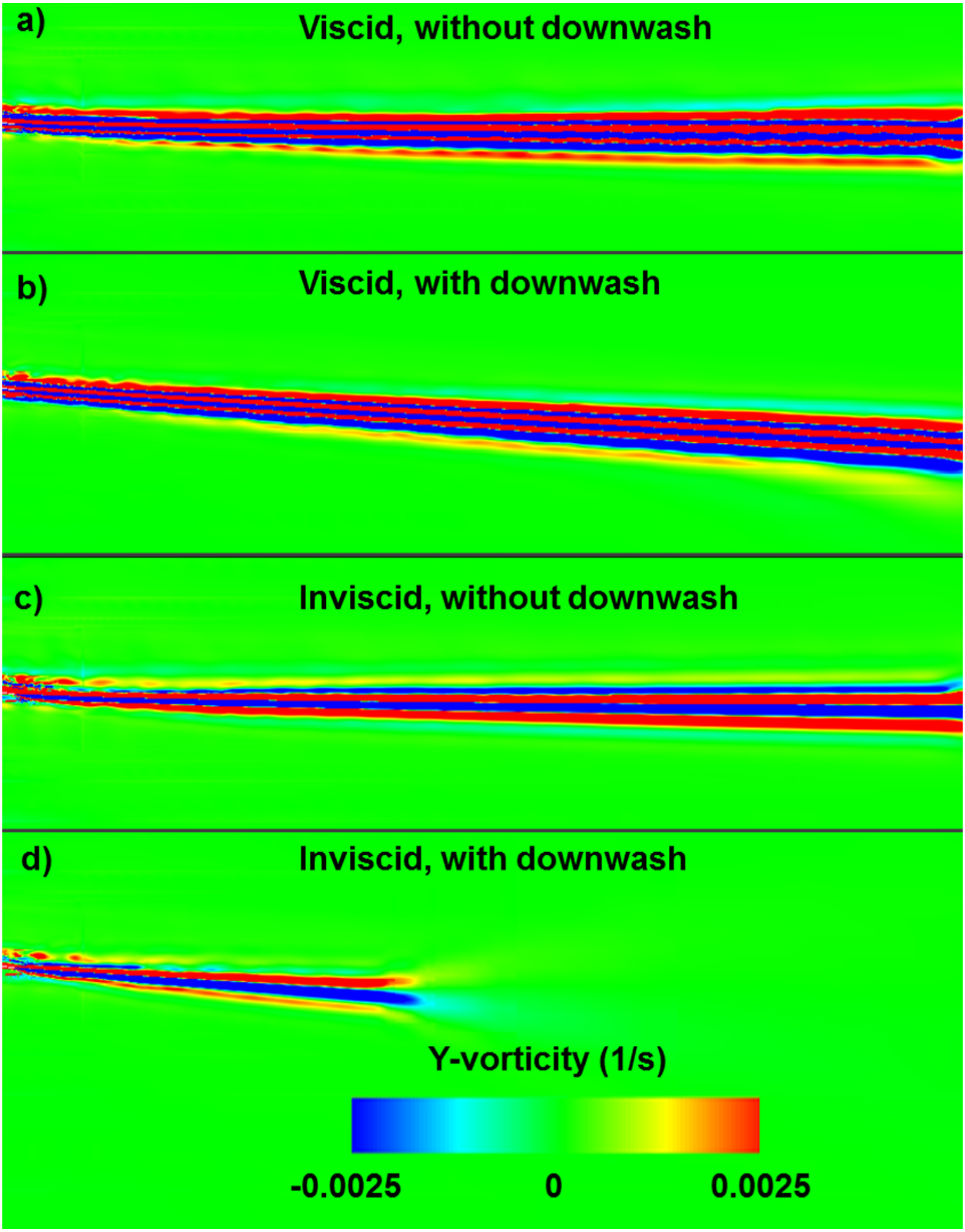

Fig. 16 An isolated NACA 0012 airfoil wake y-vorticity contour for a) viscid without downwash, b) viscid with downwash, c) inviscid, without downwash, and d) inviscid, downwash simulation (M = 0.25 (V_{tip} = 85.34 m/s), α = 9.8°, V_i = 9.45 m/s).

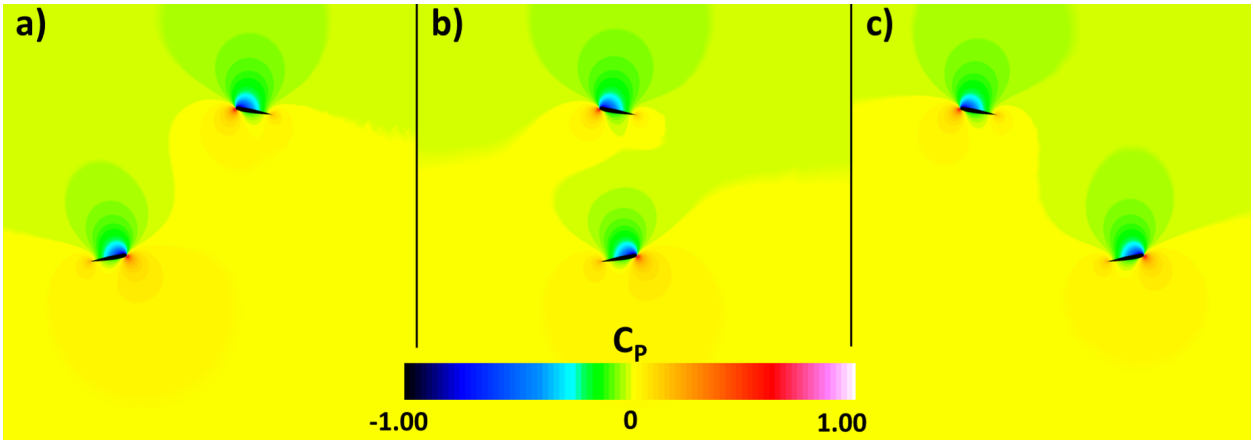

Fig. 17 A viscid flowfield C_P contour of two NACA 0012 airfoils a) before, b) at, and c) after crossing with downwash (M = 0.25 (V_{tip} = 85.34 m/s), α = 9.8°, V_i = 9.45 m/s, and S/c = 4.0 (S = 0.6096 m, c = 0.1524 m)).

Viscid flowfield C_P contours for two NACA airfoils crossing before, at, and after with downwash are shown in Fig. 17 (M = 0.25 (V_{tip} = 85.34 m/s), α = 9.8°, V_i = 9.45 m/s, and S/c = 4.0 (S = 0.6096 m, c = 0.1524 m)). As previously shown in Fig. 6 and shown in Fig. 17, as the two airfoils approach each other the flowfield between the two airfoils start to interact, which results in a change in angle-of-attack of both airfoils due to the induced velocity (see Fig. 7).

Figure 18 shows vorticity contours of the flowfield of two NACA 0012 airfoils after time of crossing. Viscid and inviscid results are shown, with and without a vertical velocity imposed (M = 0.25 (V_{tip} = 85.34 m/s), α = 9.8°, V_i = 9.45 m/s). Similar to the isolated airfoil (Fig. 16), the vortex sheet behind the airfoil travels downward due to the imposed vertical velocity (Figs. 18 b), d)).

The effect of shed vorticity is highlighted after the airfoils cross each other at the location of overlap, as shown in Fig. 18. Inviscid calculations with and without downwash reveal deposited vorticity at the location of overlap (Figs. 18 c) and d)), while viscid solutions are harder see due to the presence of viscosity (Figs. 18 a) and b)).

3. Single train of eight airfoils

When airfoils are added ahead or behind an isolated airfoil, each airfoil will encounter the wake of the preceding airfoils. Rapid changes in airfoil lift and drag due to wake interactions will result in shed vorticity deposited into the fluid medium. Any ensuing airfoils that impinge on these shed vortices are susceptible to additional airload fluctuations.

A single train of eight airfoils was simulated in order to investigate the effect of shed vorticity as depicted in Figs. 1 i), k), j), and l). A train of eight airfoils was chosen to ensure that there was sufficient aerodynamic influence from airfoils preceding and following the airfoil of interest. The 4th airfoil in the train was selected for analysis and is noted as $A4$.

Comparing $A4$ to the isolated airfoil, the difference in c_z shows an overall small decrease in lift for all inviscid and viscid calculations with and without downwash (Fig. 12), while a small increase in viscid c_x calculations is observed (Fig. 13). An overall increase in viscid c_m calculations is observed for $A4$ compared to the isolated airfoil simulations with and without downwash (Fig. 14).

Vorticity contours for $A4$ are shown in Fig. 19. The wakes from the airfoils preceding $A4$ are clearly shown in Figs. 19 a), b), and c), whereas in Fig. 19 d) the wakes are not seen. The presence of downwash pushes the wake from the preceding two ($A2$, $A3$) airfoils into proximity of $A4$ (Fig. 19 b)) so the wake is not seen in the inviscid simulation (Fig. 19 d)) due to the absence of viscosity.

4. Two trains of eight airfoils crossing

The final configuration studied was two eight-airfoil trains. The addition of the second train should capture all effects explored thus far: circulation, thickness, compressibility, viscosity, and downwash. The 4th airfoils of the upper train and lower train, $UA4$ and $LA4$, respectively, were analyzed. The two airfoils, $UA4$ and $LA4$, experienced lower lift, higher drag and higher moment compared to the case of two airfoils (UA, LA) crossing, with and without downwash (Figs. 12 through 14). As $UA4$ and $LA4$ encounter an overlap, the deposited shed vorticity builds upon

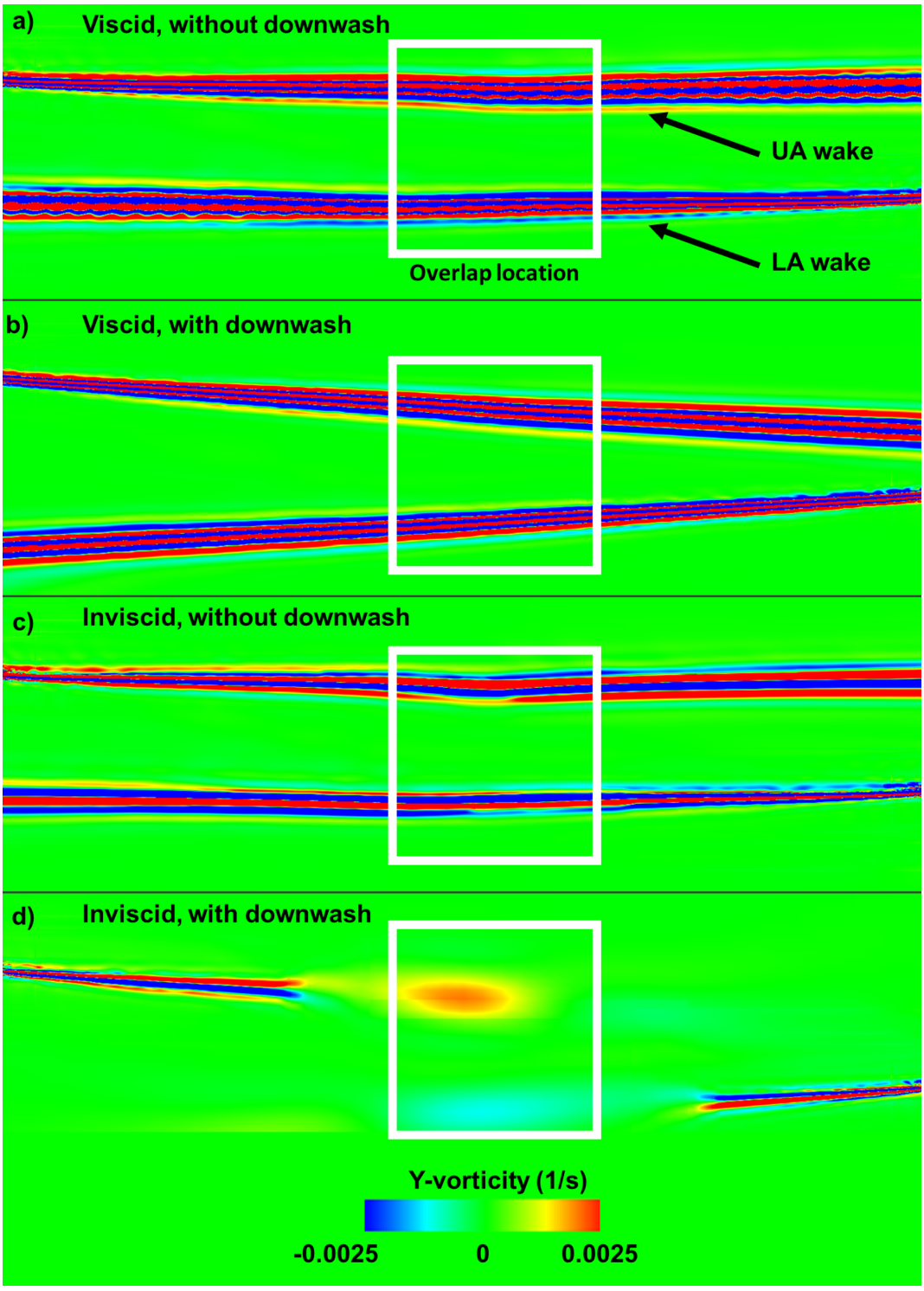

Fig. 18 Two NACA 0012 airfoils y-vorticity contour after time of crossing for a) viscid without downwash, b) viscid with downwash, c) inviscid, without downwash, and d) inviscid, downwash simulation (M = 0.25 (V_{tip} = 85.34 m/s), α = 9.8°, V_i = 9.45 m/s, and S/c = 4.0 (S = 0.6096 m, c = 0.50)).

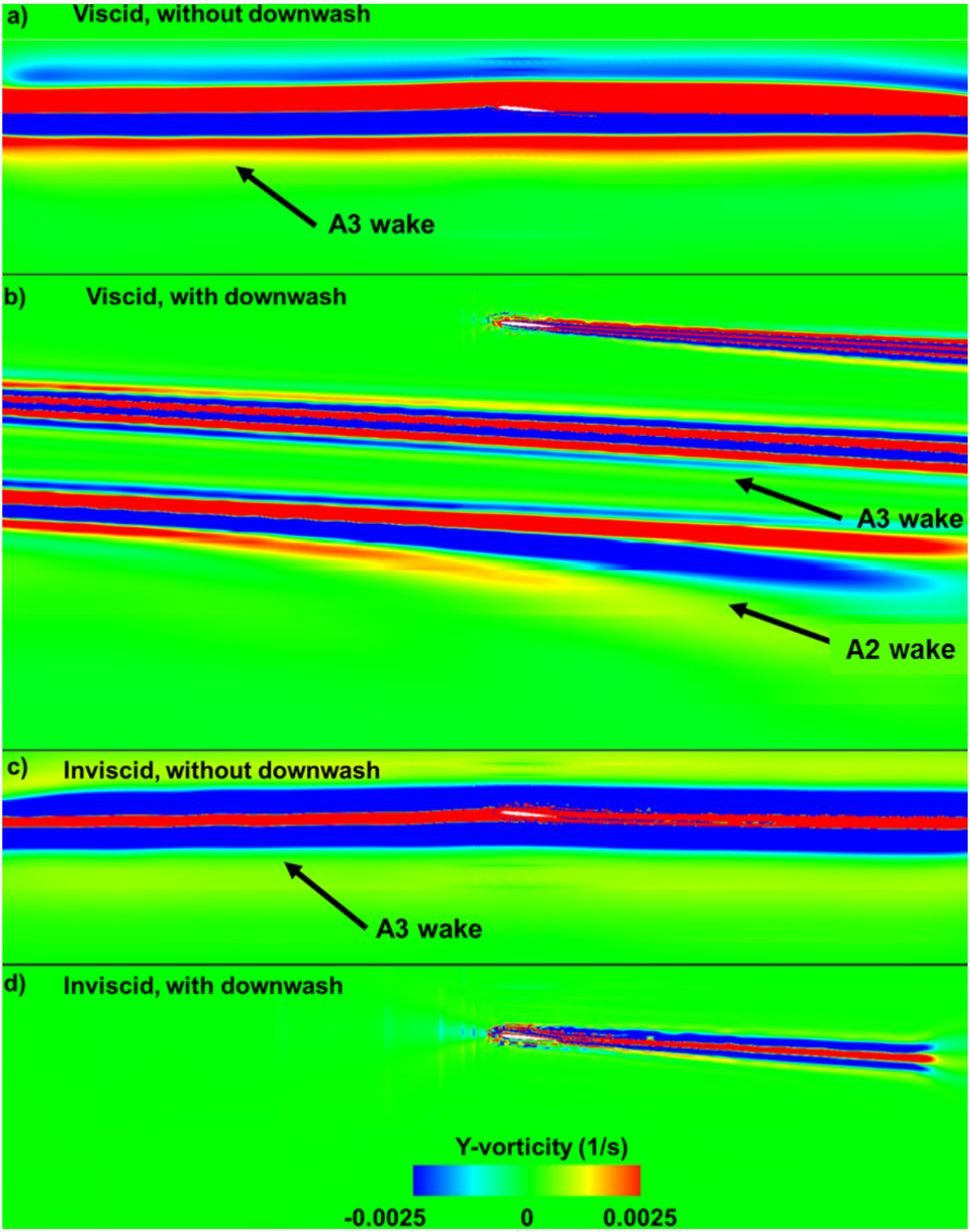

Fig. 19 Vorticity contours for $A4$ (4th airfoil in a train of eight airfoils) for a) viscid no downwash, b) viscid with downwash, c) inviscid, without downwash, and d) inviscid, downwash simulation (M = 0.25, α = 9.8°,V_i = 9.45 m/s, and D/c = 33.51).

previous deposited shed vorticity from overlapping occurrences, resulting in lower lift, higher drag and higher moment.

A comparison of vorticity fields of UA/LA and $UA4/LA4$ with downwash is shown in Figs. 20 a) and b), respectively. The addition of airfoils further complicates the flow. Although the downwash pushes the wake and deposited shed vorticity downward, in Fig. 20 b) the oncoming lower airfoil ($LA4$) encounters the wake of $UA3$. Figure 21 shows c_z versus distance to overlap of $UA4$ and $LA4$, where $UA4$ and $LA4$ are overlapping $LA1$-$LA8$ and $UA1$-$UA8$, respectively. Also shown in Fig. 21 are viscid calculations with downwash for an isolated airfoil (ISO), two airfoils crossing (UA,LA), and a single train of eight airfoils crossing ($A4$). Comparing $UA4$ and $LA4$ to the other simulations, the mean lift decreases after each overlapping occurrence. The decrease in lift is due to the deposited shed vorticity, where the shed vorticity from $UA3$ interacts with $LA4$ and increases the angle of attack.

VI. Conclusion

A potential and compressible flow computational code was used to understand coaxial rotor specific aerodynamic phenomena in 2D. The potential code VITS (Vortex Interaction Tracking Simulation) was used to understand the flowfield during a blade crossing event where compressibility and downwash are not accounted for. VITS revealed that the lift of both the upper and lower airfoil increased before overlap followed by a decrease in lift after overlap. Before overlap, the upper airfoil sees an increase in angle-of-attack due to the upwash from the lower airfoil, while the opposite occurs after overlap.

OVERFLOW 2.2k was used to model an isolated airfoil, two airfoils crossing, single train of eight airfoils, and two trains of eight airfoils crossing. Previously, the crossing of two airfoils in 2D, offset vertically and traveling in opposite directions were simulated while the angle-of-attack, airfoil thickness, vertical spacing between the airfoils, and Mach number (including transonic and compressible cases) were individually varied to isolate the effects of circulation, thickness, and compressibility. To dissect the effect of downwash and shed vorticity, an isolated airfoil, two airfoils crossing, single train of eight airfoils, and two trains of eight airfoils crossing were simulated to isolate each effect. Downwash was simulated by introducing a vertical velocity. Furthermore, the difference between viscid and inviscid solutions were compared to understand the effect of shed vorticity from a blade crossing event.

The effect of downwash resulted in a decrease in lift for all viscid and inviscid calculations. For all viscid simulations, the addition of downwash increased drag and decrease moment; the increase in drag is due to the additional force vector from the downwash.

The single train of eight airfoils showed negligible differences in lift, drag, and moment compared to the isolated airfoil and a greater difference is observed when comparing the two trains of eight airfoils crossing due to the presence of deposited shed vorticity at the location of overlap. For the two trains of eight airfoils crossing simulation, the presence of airfoils ahead and behind each other is significant due to the presence of shed vorticity in terms of lift, drag, and moment.

Downwash causes the shed vorticity of the upper airfoils to interact with the lower airfoils, reducing the angle of attack of the lower airfoils. As a result, the lift of the lower airfoils is decreased and the drag is increased.

References

[1] Coleman, C. P., "A Survey of Theoretical and Experimental Coaxial Rotor Aerodynamic Research," NASA TP- 3675, NASA, March 1997.

[2] Barbely, N. L., Komerath, N. M., and Novak, L. A., "A Study of Coaxial Rotor Performance and Flow Field Characteristics," *American Helicopter Society Aeromechanics Specialist's Conference*, 2016.

[3] Barbely, N. L., and Komerath, N. M., "Coaxial Rotor Flow Phenomena in Forward Flight," *SAE 2016 Aerospace Systems and Technology Conference*, 2016.

[4] Barbely, N. L., and Komerath, N. M., "Compressible 2D flow field interaction of two contra-rotating blades," *SAE 2016 Aerospace Systems and Technology Conference*, 2016.

[5] Schatzman, N. L., Komerath, N. M., and Romander, E., "Time-Varying Loads of Co-Axial Rotor Blade Crossings," *SAE 2017 Aerospace Systems and Technology Conference*, 2017.

[6] Singh, P., and Friedmann, P. P., "Application of Vortex Methods to Coaxial Rotor Wake and Load Calculations," *55th AIAA Aerospace Sciences Meeting*, 2017.

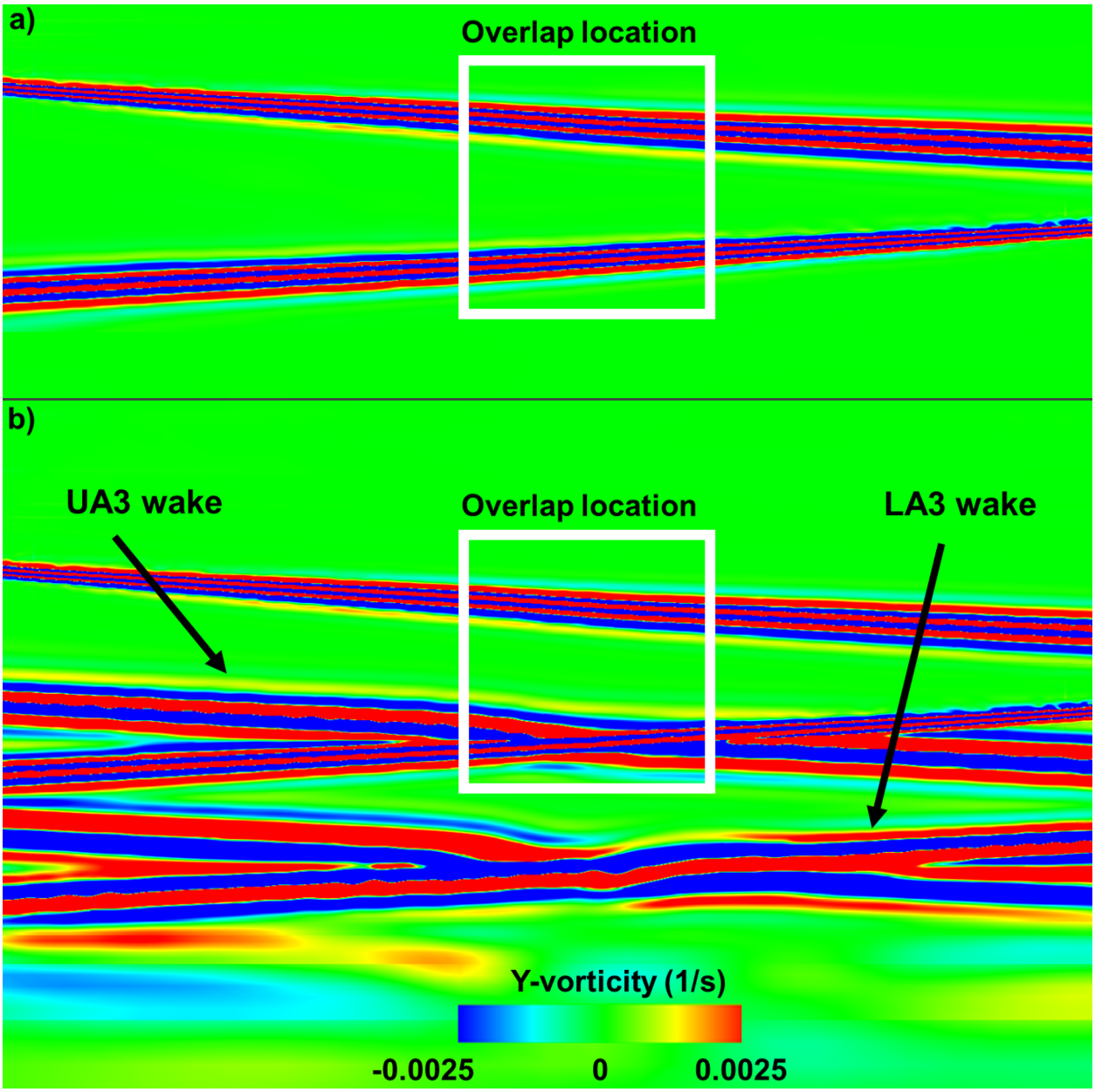

Fig. 20 Vorticity contour with downwash viscid simulation of a) two airfoils (UA/LA) crossing and b) two trains of eight airfoils crossing after time of overlap of upper and lower airfoil four ($UA4/LA4$) (M = 0.25, α = 9.8°,V_i = 9.45 m/s, S/c = 4.0 (S = 0.6096 m, c = 0.1524 m), and D/c = 33.51).

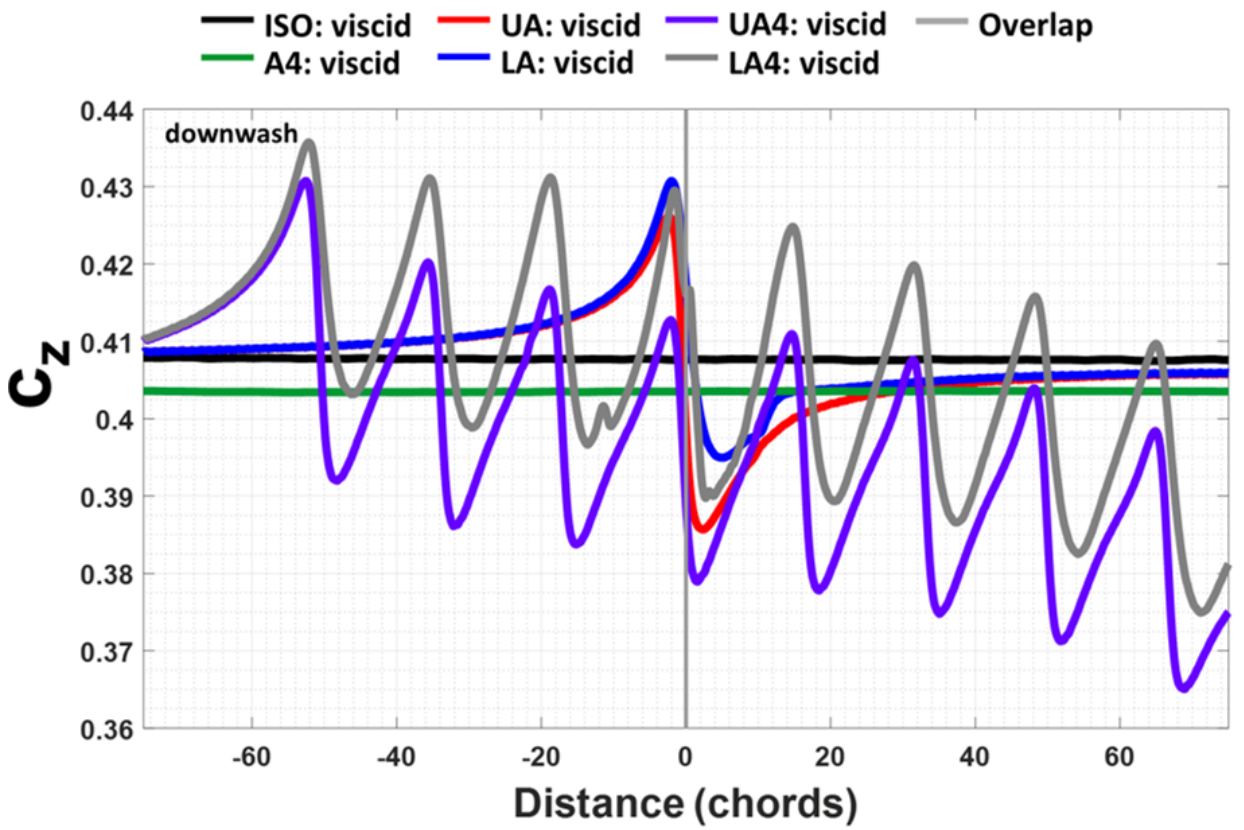

Fig. 21 Viscid calculations with downwash for an isolated airfoil, two airfoils crossing, a single train of eight airfoils crossing ($A4$), and two trains of eight airfoils crossing ($UA4$ and $LA4$), c_z versus distance to overlap (M = 0.25, α = 9.8°, V_i = 9.45 m/s, S/c = 4.0 (S = 0.6096 m, c = 0.1524 m), and D/c = 33.51).

[7] Feil, R., Rauleder, J., Hajek, M., Cameron, C., and Sirohi, J., "Computational and Experimental Aeromechanics Analysis of a Coaxial Rotor System in Hover and Forward Flight," *Proceedings of the 42nd European Rotorcraft Forum, Lille, France*, 2016.

[8] Schmaus, J. H., and Chopra, I., "Aeromechanics of Rigid Coaxial Rotor Models for Wind-Tunnel Testing," *Journal of Aircraft*, Vol. 54, No. 4, 2017.

[9] Cameron, C. G., Uehara, D., and Sirohi, J., "Transient Hub Loads and Blade Deformation of a Mach-Scale Coaxial Rotor in Hover," *AIAA Science and Technology Forum and Exposition, SciTech*, 2015.

[10] Cameron, C. G., A., K., and Sirohi, J., "Performance of a Mach-Scale Coaxial Counter-Rotating Rotor in Hover," *Journal of Aircraft,*, Vol. 53, No. 3, 2016, pp. 746–755.

[11] Johnson, W., "Influence of Lift Offset on Rotorcraft Performance," NASA TP- 215404, NASA, 11 2009.

[12] Bertin, J. J., and Smith, M. L., *Aerodynamics for engineers*, Prentice-Hall, 1998.

[13] Nichols, R., and Buning, P., "User's Manual for OVERFLOW 2.2," *NASA Langley Research Center, Hampton, VA, Aug*, 2010.

[14] Johnson, W., *CAMRAD-II: Comprehensive Analytical Model for Rotorcraft Aerodynamics and Dynamics*, Johnson Aeronautics, 2007.

[15] Leishman, J. G., and Ananthan, S., "An optimum coaxial rotor system for axial flight," *Journal of the American Helicopter Society*, Vol. 53, No. 4, 2008, pp. 366–381.

[16] Harrington, R. D., "Full-scale-tunnel investigation of the static-thrust performance of a coaxial helicopter rotor," NACA TN-2318, NACA, 3 1951.